European Journal of Medicinal Chemistry 219 (2021) 113428

Contents lists available at ScienceDirect

European Journal of Medicinal Chemistry

journal homepage: http://www.elsevier.com/locate/ejmech

Research paper

Ring-opening of five-membered heterocycles conjugated 4-isopropylresorcinol scaffold-based benzamides as HSP90 inhibitors suppressing tumor growth *in vitro* and *in vivo*

Yi-Min Liu [a, b, 1], Huang-Ju Tu [c, 1], Chueh-Heng Wu [e, 1], Mei-Jung Lai [b, d], Shu-Chieh Yu [a], Min-Wu Chao [c], Yi-Wen Wu [c], Che-Ming Teng [e], Shiow-Lin Pan [b, c, d, **], Jing-Ping Liou [a, b, d, *]

[a] School of Pharmacy, College of Pharmacy, Taipei Medical University, 250 Wuxing Street, Taipei, 11031, Taiwan
[b] Biomedical Commercialization Center, Taipei Medical University, Taipei, 11031, Taiwan
[c] Graduate Institute of Cancer Molecular Biology and Drug Discovery, College of Medical Science and Technology, Taipei Medical University, Taipei, 11031, Taiwan
[d] Ph.D. Program in Drug Discovery and Development Industry, College of Pharmacy, Taipei Medical University, Taipei, 11031, Taiwan
[e] Pharmacological Institute, College of Medicine, National Taiwan University, Taipei, Taiwan

ARTICLE INFO

Article history:
Received 13 November 2020
Received in revised form
12 March 2021
Accepted 29 March 2021
Available online 6 April 2021

Keywords:
Ring-opening
Heat shock protein 90 inhibitors
Lung cancer

ABSTRACT

A series of ring-opened dihydroxybenzamides have been designed and synthesized as heat shock protein 90 inhibitors. One of derivatives, compound **6b** ((*N*-ethyl-2,4-dihydroxy-5-isopropyl-*N*-(pyridin-3-yl) benzamide)) demonstrated remarkable antiproliferative activity against in human KRAS mutant A549 and EGFR T790 M mutant H1975 lung cancer cell lines with GI_{50} values of 0.07 and 0.05 μM, respectively. It is also active against in other cancer cell lines, such as colorectal HCT116 (GI_{50} = 0.09 μM), liver Hep3B (GI_{50} = 0.20 μM) and breast MDA-MB-231 (GI_{50} = 0.09 μM), and shows no evidence of toxicity in normal cell line. Compound **6b** has an IC_{50} of 110.18 nM in HSP90α inhibitory activity, slightly better than reference compound **1** (17-AAG, IC_{50} = 141.62 nM) and achieves the degradation of multiple HSP90 client proteins in a dose- and time-dependent manner and downstream signaling of Akt in a concentration- and time-dependent manner in the human A549 lung cancer cell line. In the Boyden chamber assay, compound **6b** can efficiently inhibit the migration of A549 cells when compared to the reference compound **1**. It also induce significant activity through the apoptotic pathway. Treatment with **6b** showed no vision toxicity (IC_{50} > 10 μM) on 661w photoreceptor cells as compared to AUY922 (**3a**) with a 0.04 μM values of IC_{50} and has no effect in hERG test. In a bidirectional Caco-2 permeability assay, compound **6b** was classified as a highly permeable compound which is not a substrate of efflux transporters. In a pharmacokinetic study in rats, **6b** showed an F = 17.8% of oral bioavailability. The effect of metabolic stability of compound **6b** in human hepatocytes showed a $T_{1/2}$ of 67.59 min. Compound **6b** (50 mg/kg, po, daily) exhibits antitumor activity with a 72% TGD (tumor growth delay) in human A549 lung xenograft. The combination of **6b** and afatinib, orally administered, showed tumor growth suppression with 67.5% of TGI in lung H1975 xenograft model. Thus compound **6b** is a lead compound for further development of potential agents to treat lung cancer.

Abbreviations: DCM, dichloromethane; DMAP, 4-(Dimethylamino)pyridine; DMF, dimethylformamide; EDC . HCl, *N*-(3-Dimethylaminopropyl)-*N*′-ethylcarbodiimide hydrochloride; HOBt, 1-Hydroxybenzotriazole hydrate; NMM, *N*-methylmorpholine; TFA, trifluoroacetic acid; THF, tetrahydrofuran.

* Corresponding author. School of Pharmacy, College of Pharmacy, Taipei Medical University, 250 Wuxing Street, Taipei, 11031, Taiwan.
** Corresponding author. Biomedical Commercialization Center, Taipei Medical University, Taipei, 11031, Taiwan.
E-mail addresses: slpan@tmu.edu.tw (S.-L. Pan), jpl@tmu.edu.tw (J.-P. Liou).

[1] Authors contributed equally.

https://doi.org/10.1016/j.ejmech.2021.113428
0223-5234/

1. Introduction

Heat shock proteins (HSPs) are molecular chaperones which play an essential role in the development of proteins. They are required for basic functions like protein folding and participate in many higher-order functions such as post-translational regulation of signaling molecules and assembly or disassembly of transcriptional complexes. Heat shock proteins are classified into different families based on their molecular weight. HSPs, especially HSP90 which is associated with a number of signaling pathways [1,2], have been widely investigated in recent decades.

HSP90 has a primary role in both normal and cancer cells in activation of a wide range of proteins known as HSP90 client proteins. These client proteins can be separated into three main classes: steroid hormone receptors, tyrosine and serine/threonine kinases, and proteins with miscellaneous functions. Cancer cells overexpress a number of HSP90 client proteins, such as hypoxia-inducible factor-1α (HIF-1α), mutant p53, AKT (protein kinase B) and epidermal growth factor receptor (EGFR), which are all involved in tumor proliferation and metastasis [3,4].

HSP90 plays a pivotal role in the hallmarks of cancer cells and its inhibition and disruption can affect processes involved in the initiation of cancer. Consequently, some compounds behaving as HSP90 inhibitors have entered clinical trials. HSP90 inhibitors can be divided into several classes based on distinct structures. Examples include ansamycin derivatives as 17-AAG (**1**, Tanespimycin, Phase III) [5], purine derivatives as BIIB021 (**2**, Phase II) [6], resorcinol derivatives such as AUY922 (**3a**, Luminespib, Phase II) [7], STA-9090 (**3b**, Ganetespib, Phase III) [8] and AT-13387 (**3c**, Onalespib, Phase II) [9] (Fig. 1). Especially the resorcinol derivatives, there are few compounds under investigation with different core structures have shown significant activities and served as HSP90 inhibitors. For example, the aryl-triazolyl acetate (**4a**), tetraisoquinolinecarboxamide (**4b**), amide-tethered quinoline (**5a**), N-benzyl benzamide (**5b**) have also been reported [10] (Fig. 1).

Among HSP90 inhibitors in the clinical trials, the resorcinol derivatives are commonly used alone or in combination with proteasome inhibitors in the treatment of non-small cell lung cancer (NSCLC) and can have significant outcomes [11–14]. With the appearance of these related results, HSP90 has emerged as a notable anticancer target.

Though the use of an HSP90 inhibitor, the treatment of non-small cell lung cancer (NSCLC) has enjoyed some success, but vision-related disorders have been reported. In the Phase 2 study of the AUY922 (**3a**) in previously treated patients with advanced NSCLC for example, vision-related disorders were reported in 79.7% of patients (most were grade 1/2). 22.9% of patients reported night blindness and 22.2% of patients reported photopsia. Other vision-related disorders have also been reported, such as vision blurred (19.6%), visual impairment (19.6%), and visual acuity reduced (17.0%) [15]. In another Phase 2 study of the activity of AUY922 (**3a**) against NSCLC harboring EGFR exon 20 insertions, vision changes were reported in 76% of patients (most were grade 1/2) [16].

Because of the significant treatment outcomes and the concern of vision disorders, we investigated the concept of ring-opening in a rational design process. Compounds **3a**-**3b** (Fig. 1) possess a ring system connected to a resorcinol and compound **3c** has a ring connected to a resorcinol through an amide linker. Attempts were made to modify this ring system by introducing various aryl rings connected by an amide linker, for example, compounds **6** (3-aminopyridine), **7** (4-aminopyridine) and **8** (5-aminoindole). In addition, an attempt was also made to utilize different-sized alkyl groups in the substituents linked to resorcinol through the amide linkage, to generate a series of potential HSP90 inhibitors (Fig. 2). In this way, a number of designed target compounds (**6**–**8**) (Table 1) were synthesized and their antiproliferative activity was evaluated and discussed below.

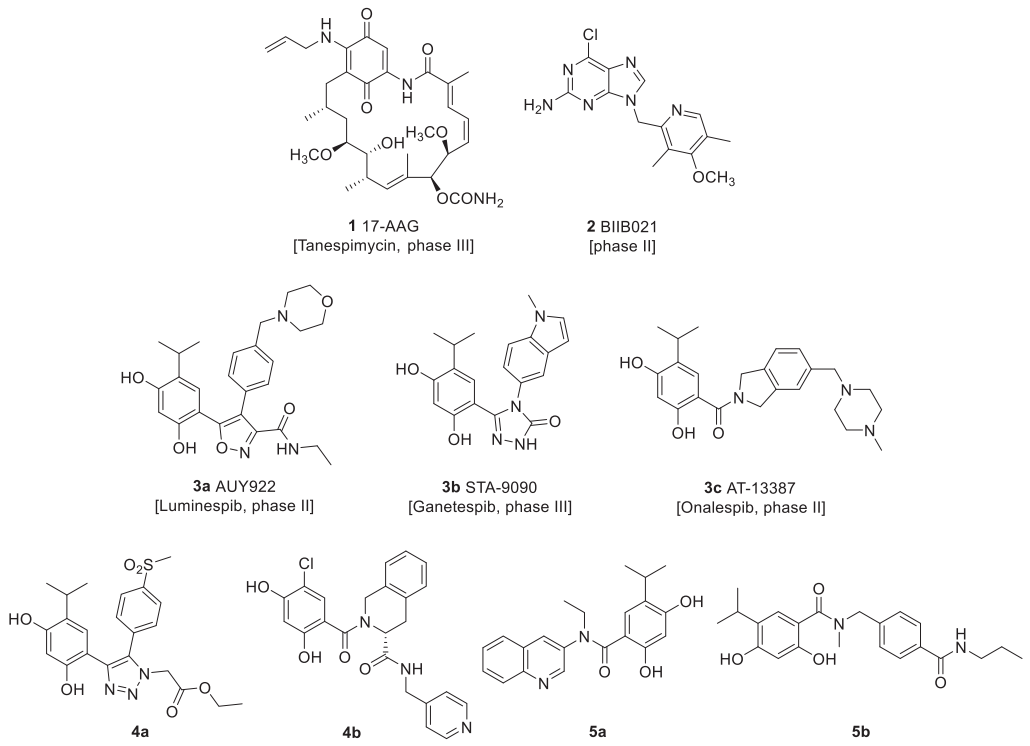

Fig. 1. Structures of HSP90 inhibitors in clinical trials and compounds under investigation.

2. Results and discussion

2.1. Chemistry

Scheme 1 shows the synthesis of compounds **6a**-**6d** and **7a**-**7d**. Compound **9** was reacted with *m*- or *p*-aminopyridine in the presence of a coupling reagent such as EDC.HCl to yield compounds **10**–**11**. The benzyl group in compounds **6a** and **7a** was removed by hydrogenolysis. The amide NH group of intermediates (**10**–**11**) was deprotonated by strong base to generate the alkylated products, then completed with the debenzylation by hydrogenolysis to afford compounds **6b**-**6d** and **7b**-**7d**.

Scheme 2 depicts the synthesis of compounds **8**. Compound **12** is commercially available and was reacted with Boc anhydride or methyl iodide to attack the N-1 position of indole, followed by reduction of the nitro group and an amide coupling reaction with compound **9** to yield intermediates **13**–**14**. The protecting groups in compounds **8a** and **8f** were directly removed treatment with acid or heterolytic H_2 cleavage. Compounds with an alkyl group at the amide linkage (**8b**-**8e** and **8g**-**8i**) were used in similar synthetic procedures.

Synthesis of the intermediate compound (**9**) began from compound **15**, which is commercially available, and proceeded through five steps to yield the product (Scheme 3). First, the hydroxyl groups of compound **15** were protected by benzyl groups (**16**). Next, the acetyl group was converted to a tertiary alcohol (**17**) by a Grignard reaction and then reacted with triethylsilane and TFA to get compound **18**. Finally, to undergo formylation with the Vilsmeier reaction (**19**) and then oxidation, compound **19** was converted to the intermediate compound **9**.

Table 1
Structures of designed and synthesized compounds (**6**–**8**).

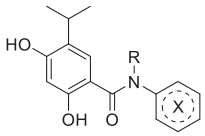

R= H, akyl group
6 X= 3-aminopyridine
7 X= 4-aminopyridine

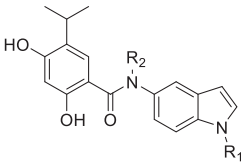

R_1, R_2= H, akyl group
8

	R		R_1	R_2
6a	H	**8a**	H	H
6b	C_2H_5	**8b**	H	CH_3
6c	C_3H_7	**8c**	H	C_2H_5
6d	$CH(CH_3)_2$	**8d**	H	C_3H_7
7a	H	**8e**	H	$CH(CH_3)_2$
7b	C_2H_5	**8f**	CH_3	H
7c	C_3H_7	**8g**	CH_3	CH_3
7d	$CH(CH_3)_2$	**8h**	CH_3	C_2H_5
		8i	CH_3	C_3H_7

2.2. Biological evaluation

2.2.1. In vitro cell growth inhibitory activity

The synthetic compounds (**6**–**8**) were evaluated for their

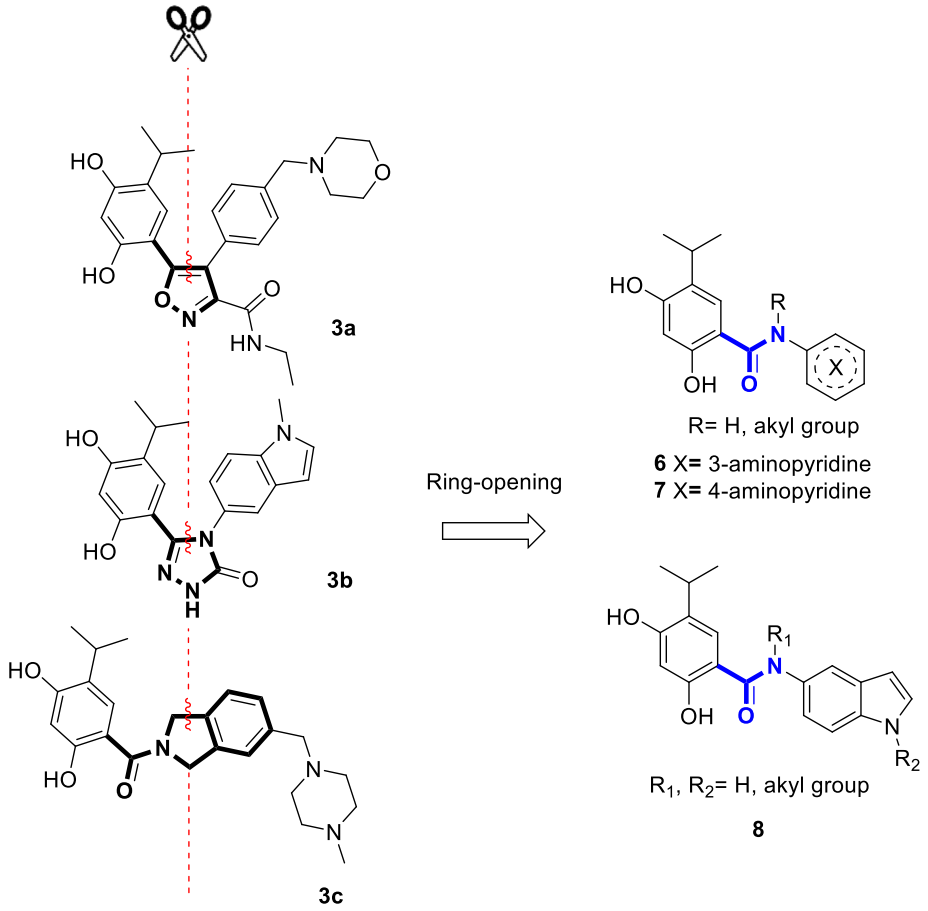

Fig. 2. The rational design of compounds **6**–**8** with the ring-opening concept.

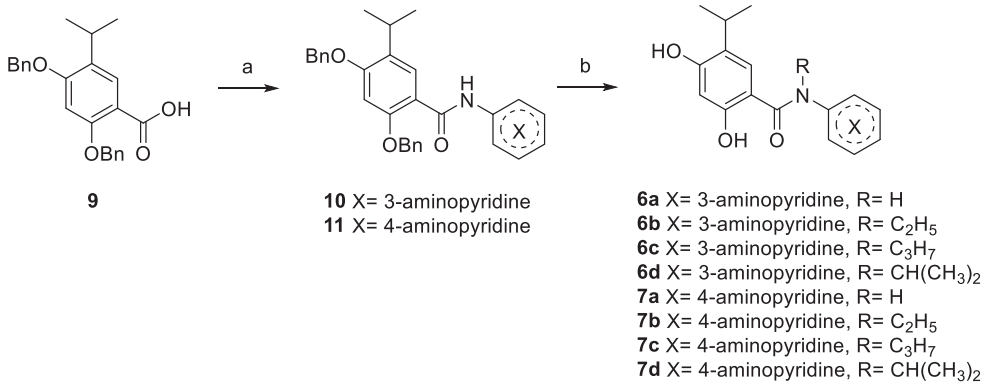

Scheme 1. Synthetic route to compounds **6**-**7**[a]. [a]Reagents and conditions: (a) 3-or 4-aminopyridine, EDC.HCl, HOBt, NMM, DMF, r.t., 71–73%; (b) for **6a** and **7a**, 10% Pd/C, H_2, MeOH, r.t., 87–88%; for **6b**-**6d** and **7b**-**7d**, alkyl iodide, NaH, DMF, r.t. then 10% Pd/C, H_2, MeOH, r.t., 60–70%.

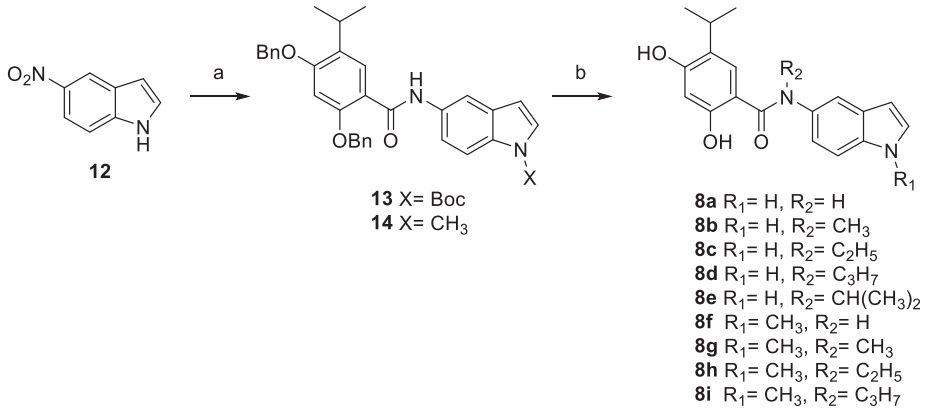

Scheme 2. Synthetic route to designed compounds **8**[a]. [a]Reagents and conditions: (a) (i) for **13**, Boc anhydride, DMAP, DCM, r.t.; for **14**, methyl iodide, NaH, DMF, r.t.; (ii) Fe powder, NH_4Cl, IPA/H_2O, reflux, (iii) **9**, EDC.HCl, HOBt, NMM, DMF, r.t., 33–79% in three steps; (b) for **8a**, (i) TFA, DCM, r.t. (ii) 10% Pd/C, H_2, MeOH, r.t., 73% in two steps; for **8b**-**8e**, (i) alkyl iodide, NaH, DMF, r.t. (ii) TFA, DCM, r.t. (iii) 10% Pd/C, H_2, MeOH, THF, 40 psi, r.t., 48–57% in three steps; for **8f**, 10% Pd/C, H_2, MeOH, r.t., 48%; for **8g**-**8i**, (i) alkyl iodide, NaH, DMF, r.t., (ii) 10% Pd/C, H_2, MeOH, r.t., 71–75% in two steps.

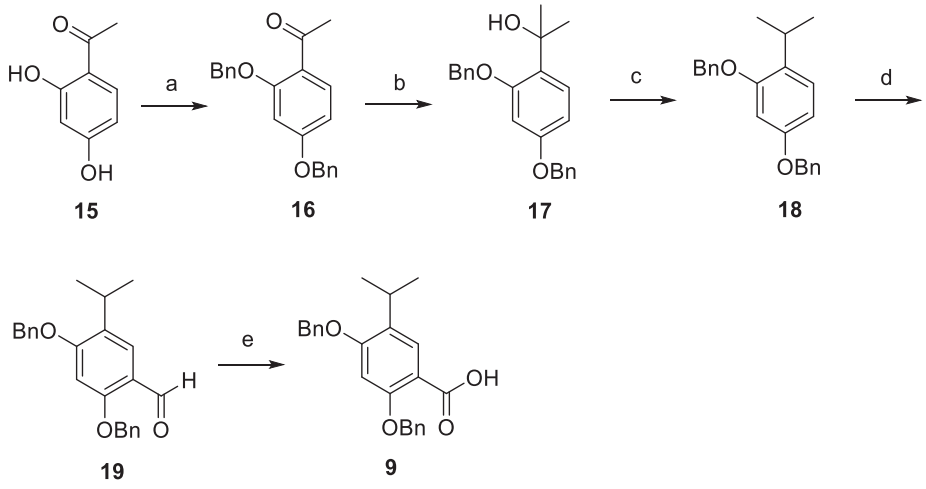

Scheme 3. Synthetic route to intermediate compound **9**[a]. [a]Reagents and conditions: (a) benzyl bromide, K_2CO_3, acetone, reflux, 93%; (b) methylmagnesium bromide, THF, 0 °C to r.t., 77%; (c) triethylsilane, TFA, DCM, −78 °C to r.t., 92%; (d) $POCl_3$, DMF, 0 °C–80 °C, 92%; (e) sulfamic acid, $NaClO_2$, H_2O, THF, dimethyl sufoxide, 0 °C to r.t., 65%.

antiproliferative activity against human A549 lung cancer cell line (Table 2). Based on the activity results, compounds such as **6a**, **7a**, **8a** and **8f** with a free amide linkage displayed loss of activity. The varying carbon length of alkyl groups in the substituted amide linkage exhibits a regular pattern in the growth inhibitory activity. The inhibitory activity increases with a methyl group (**8b**, **8g**) or an

ethyl group (**6b**, **7b**, **8c**, **8h**), but decreases with a propyl group (**6c**, **7c**, **8d**, **8i**) or an isopropyl group (**6d**, **7d**, **8e**). Interestingly, compounds with an ethyl-substituted amide linkage (**6b**, **7b**, **8c**, **8h**) show the best antiproliferative activity in every series. Amongst the synthetic compounds (**6**–**8**), compound **6b** shows significant inhibitory activity against to A549 cancer cell line with GI_{50} value of 0.07 ± 0.01 μM.

2.2.2. Antiproliferative activity and HSP90 enzyme inhibition against normal and cancer cell lines

We sought to learn if these synthetic compounds also possess antiproliferative activity and HSP90 enzyme inhibition in other cancer cell lines and the results are shown in Table 3. We chose to investigate compounds **6b**, **7b**, **8b**, **8c** and **8g,** which possess good antiproliferative activity against the A549 lung cancer cell line. Compound **6b** has exhibited similar activity in human HCT116 colorectal cancer cell line (0.09 ± 0.01 μM) and MDA-MB-231 breast cancer cell line (0.09 ± 0.01 μM) compared to that of the A549 cell line and slightly decreased activity against the Hep3B hepatocellular carcinoma cell line (0.20 ± 0.01 μM). In addition, the inhibitory activity of compound **6b** is also better than the reference compounds **1** (17-AAG) and **2** (BIIB021). Moreover, compound **6b** shows no evidence of toxicity in normal cell line.

Compound **6b** also possesses the best therapeutic index among these compounds with a value of 12.4 and an IC_{50} value of 110.18 ± 3.13 nM for the HSP90 enzyme inhibition which is similar to that of reference compound **2** (BIIB021) (105.06 ± 7.75 nM). These data imply that compound **6b**, with remarkable inhibitory activity against several cancer cell lines has potential for further development and it was thus selected for further investigations as an HSP90 inhibitor.

2.2.3. Evaluation of compound *6b* in degradation of HSP90 client proteins and downstream signaling of Akt

The *in vitro* western immunoblotting assay was used to confirm the mechanism of action of compound **6b** as an HSP90 inhibitor (Fig. 3). The results reveal that compound **6b** triggers the degradation of multiple HSP90 client proteins such as FAK and Src along with concomitant induction of HSP70 protein in a dose- and time-dependent manner in the human A549 lung cancer cell line (Fig. 3A and B). In addition, compound **6b** can also trigger degradation of downstream signaling of Akt in a concentration- and time-dependent manner (Fig. 3C and D). These results are consistent with the signature features of HSP90 inhibition.

2.2.4. Evaluation of compound *6b* against mutant cancer lines

Based on recent reports of increasing resistance, we have investigated if compound **6b** can act against mutant cancer cell lines (Fig. 4). Compound **6b** can induce EGFR degradation and strongly suppresses the MAPK pathways in K-ras mutant A549 cancer cell line in a concentration- and time-dependent manner (Fig. 4A and B). As well as in human H1975 lung cancer cell line, which is a T790M-positive cell line harboring the EGFR L858R/T790 M double mutation, the compound **6b** was tested for inhibitory activity and showed a GI_{50} value of 0.05 ± 0.01 μM.

Table 2
Antiproliferative activity (GI_{50}) of synthetic compounds **6**–**8**.

Compound	A549 (GI_{50} ± SD[a], μM)	Compound	A549 (GI_{50} ± SD[a], μM)
6a	>10	**8a**	>10
6b	0.07 ± 0.01	**8b**	0.17 ± 0.01
6c	0.39 ± 0.01	**8c**	0.11 ± 0.01
6d	0.26 ± 0.02	**8d**	0.14 ± 0.02
7a	>10	**8e**	0.21 ± 0.02
7b	0.12 ± 0.01	**8f**	>10
7c	0.37 ± 0.05	**8g**	0.28 ± 0.02
7d	0.19 ± 0.03	**8h**	0.08 ± 0.01
		8i	0.30 ± 0.01

[a] SD: standard deviation, all experiments were independently performed at least three times.

2.2.5. Evaluation of compound *6b* on inhibition of migration

Cancer metastasis is an important issue due to the migration or invasion of neoplastic cells from the primary tumor to distant parts of the body. Herein, we have examined the anti-migration effect of compound **6b** by a Boyden chamber assay (Fig. 5). The results revealed that at 1 μM, compound **6b** can efficiently inhibit the migration of A549 cells as compared to the reference compound, **1** (**17-AAG**).

2.2.6. Evaluation of compound *6b* in cell cycle progression and apoptotic pathways

The effect of compound **6b** on cell cycle distribution was investigated by Western blotting. The data show that compound **6b** increases the expression of cyclin B1 and enhances the phosphorylation of cdc2 at Thr161 while suppressing phosphorylation of cdc2 at Tyr15 and cdc25c at Ser216 (Fig. 6A). Furthermore, the mitotic markers p-MPM-2 and p-H3 (Ser10) are also increased by compound **6b**. These results indicated that compound **6b** induces M stage arrest in A549 cells. We also found that the levels of p53 are markedly increased after cells are treated with compound **6b** or compound **1** (Fig. 6B). This overexpressed-p53 caused caspase-3, caspase-6, caspase-7, caspase-9 cleavage and induced PARP activation. Fig. 6C shows that the accumulation of p53 started at 6 h, while the activation of caspase and PARP started at 18 h. Ectopic expression of WT-p53 partially reduced caspase-3 cleavage and rescued the cell apoptosis which was caused by compound **6b** (Fig. 6D).

2.2.7. Evaluation of compound *6b* with respect to vision-related toxicity

As mentioned above, vision-related disorders of HSP90 inhibitors have been reported. In order to confirm whether compound **6b** induces vision-related toxicity, we have tested the compound **6b** on 661W photoreceptor cells (Table 4). Both compound **3a** (AUY922) and geldanamycin (an ansamycin-related HSP90 inhibitor) have displayed significantly toxicity in 661W cells with IC_{50} values of 0.04 and 1.65 μM, respectively. However, compound **6b** has an IC_{50} value over 10 μM, which indicates little or no cytotoxicity to photoreceptor cells.

2.2.8. Evaluation of compound *6b* with a potassium channel hERG test

hERG channels are involved in cardiac action potential repolarization. Inhibition of the hERG current can cause QT interval prolongation resulting in potentially fatal ventricular tachyarrhythmia. A number of drug candidates have been withdrawn from safety studies due to these cardiotoxic effects, and it is important to examine compounds for activity on hERG channels early in the lead optimization process. In order to evaluate the effect of hERG test, compound **6b** (10 μM) was conducted by the Eurofin Cerep Panlabs. The results showed the safety of compound **6b** which failed to reduce the hERG function (Table 5).

2.2.9. Evaluation of compound *6b* by CYP inhibition and permeability assays

Cytochrome P450s (CYP) are a family of enzymes which play a major role in the metabolism of drugs. Inhibition of CYPs by co-administered drugs is one of the most common causes of drug-drug interaction and leads to substantial increase of the parent

Table 3
In vitro efficacy of synthetic compounds **6b**, **7b**, **8b**, **8c** and **8g**.

Compounds	Lung A549	Colorectal HCT116	Liver Hep3B	Breast MDA-MB-231	HUVEC	TI[b]	HSP90 IC_{50} (nM)
	(GI_{50} ± SD[a], μM)						
6b	0.07 ± 0.01	0.09 ± 0.01	0.20 ± 0.03	0.09 ± 0.01	0.87 ± 0.01	12.4	110.18 ± 3.13
7b	0.12 ± 0.01	0.64 ± 0.41	0.10 ± 0.01	0.08 ± 0.01	<0.1	0.8	109.23 ± 5.35
8b	0.17 ± 0.01	1.00 ± 0.49	0.18 ± 0.04	0.07 ± 0.01	0.57 ± 0.02	3.4	115.39 ± 10.66
8c	0.11 ± 0.01	0.37 ± 0.05	0.11 ± 0.02	0.08 ± 0.01	<0.1	0.9	117.34 ± 9.62
8g	0.28 ± 0.02	0.70 ± 0.06	0.57 ± 0.32	0.10 ± 0.02	0.82 ± 0.03	2.9	105.54 ± 7.58
1 (17-AAG)	0.08 ± 0.01	0.34 ± 0.06	0.08 ± 0.01	0.27 ± 0.01	<0.1	1.3	141.62 ± 12.75
2 (BIIB021)	0.26 ± 0.03	0.25 ± 0.02	0.24 ± 0.02	0.24 ± 0.01	1.42 ± 0.09	5.5	105.06 ± 7.75

[a] SD: standard deviation, all experiments were independently performed at least three times.
[b] TI: Therapeutic Index. (HUVEC divided by the cancer cell line IC_{50}).

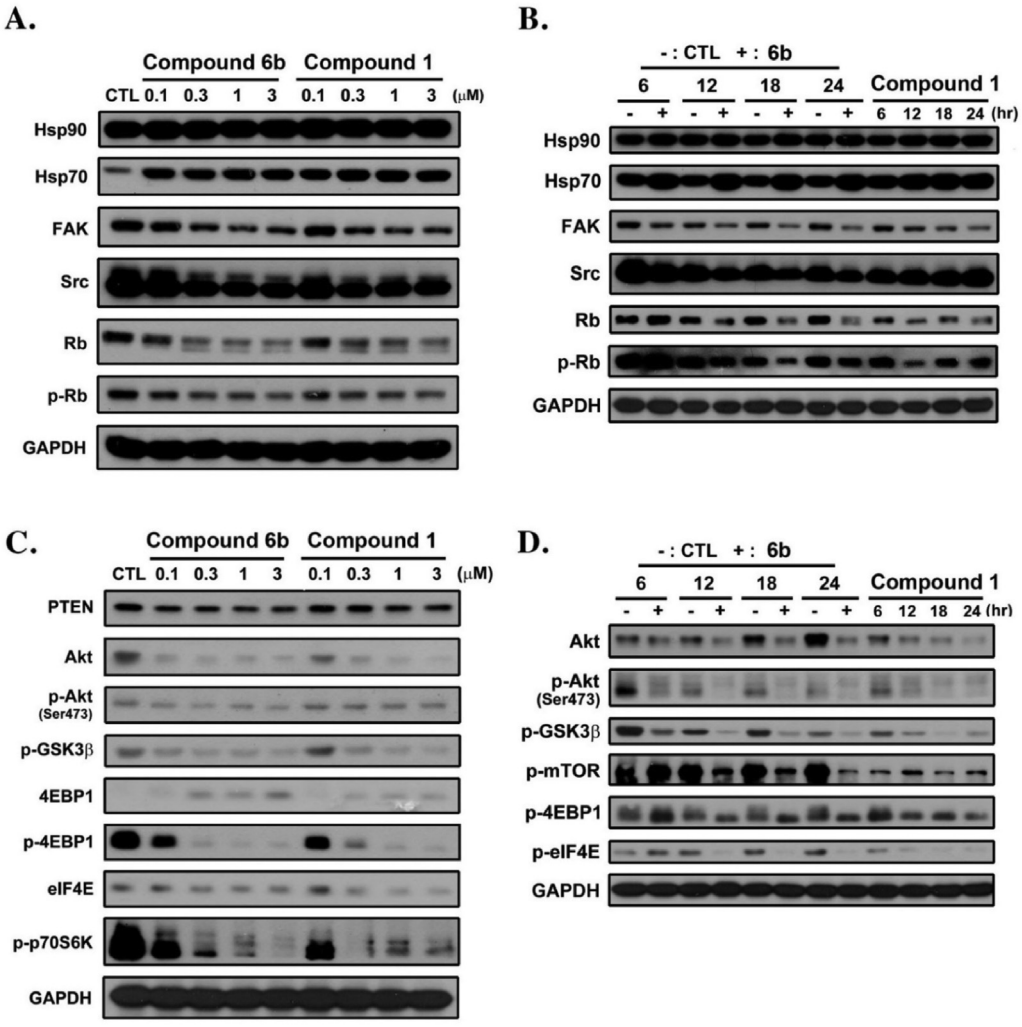

Fig. 3. Compound **6b** and compound **1** triggered degradation of multiple HSP90 client proteins and signaling downstream of Akt in a concentration- and time-dependent manner. (A, C) A549 cells were treated with DMSO or 0.1–3 μM of drugs (compound **6b** or compound **1**) for 24 h. (B, D) A549 cells were treated with 0.3 μM of indicated drugs for indicated times.

drug concentration. Compound **6b** was tested for its CYP inhibitory potential for CYP1A2, 2B6, 2C8, 2C9, 2C19, 2D6 and 3A4 (Table 6). In direct CYP inhibition assays, compound **6b** most potently inhibited CYP3A4 with IC_{50} values of 1.15 and 3.23 μM, using a substrate of

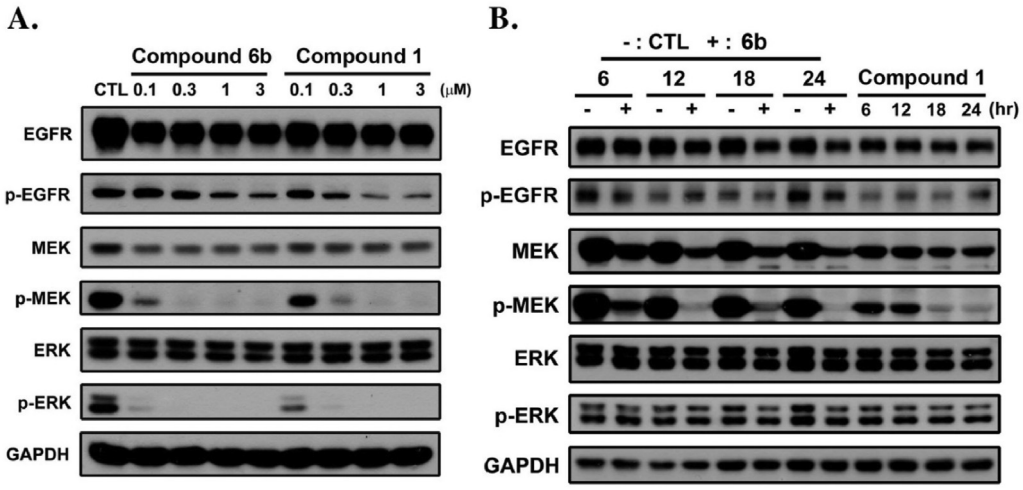

Fig. 4. Compound **6b** and compound **1** induced EGFR degradation and strongly suppressed MAPK pathways in K-ras mutant A549 cancer cell line in a concentration- and time-dependent manner. (A) A549 cells were treated with DMSO or 0.1–3 μM of drugs (compound **6b** or compound **1**) for 24 h. (B) A549 cells were treated with 0.3 μM of indicated drugs for indicated times.

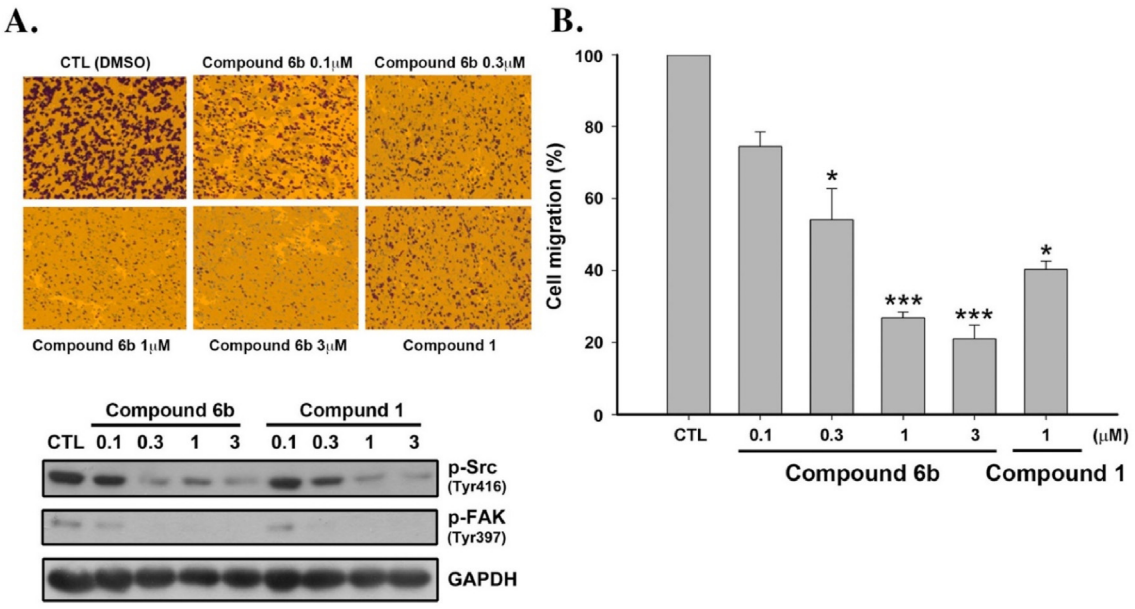

Fig. 5. Evaluation of inhibition of migration by Boyden chamber assay. (A) A549 cells were seeded in the upper compartment of the Boyden chamber (1×10^5 cells), and incubated with DMSO (CTL), 0.1–3 μM compound **6b** or 1 μM 17-AAG for 6 h. 10% FBS was placed in the lower chamber as a chemo-attractant. Migrated cells in the lower compartment were fixed, stained with crystal violet and viewed by microscopy. Two lanes of immunoblotting below were conducted to observe the inhibition of phosphorylation of Src or FAK. (B) Bar graph represents the percentage of cell migration. *$p < 0.05$, **$p < 0.01$, and ***$p < 0.001$ as compared with the control group.

testosterone and midazolam. This was followed by CYP2C19 (7.80 μM), CYP2C9 (14.97 μM), and CYP2B6 (37.17 μM). Compound **6b** partially inhibited CYP1A2, 2C8 and 2D6 with IC_{50} values > 50 μM.

A bidirectional Caco-2 permeability assay was used to examine the *in vitro* permeability of compound **6b** (Table 7). Verapamil and atenolol, with high and low permeability respectively, served as reference compounds. The Caco-2 cell permeability coefficients for apical to basolateral (AP→BL) movement and basolateral to apical (BL→AP) movement of compound **6b** were 31.9 ± 5.1 × 10^{-6}cm/s and 30.6 ± 2.1 × 10^{-6}cm/s and compound **6b** can be classified as a highly permeable compound ($P_{app,A\rightarrow B} > 10 \times 10^{-6}$ cm/s) (Table 7). It has an efflux ratio (ratio of BL→AP/AP→BL) of 0.96 and might not be a substrate of efflux transporters.

2.2.10. *Pharmacokinetics profile and metabolic stability of compound **6b***

The pharmacokinetic parameters of compound **6b** after a subsequent single intravenous (IV) administration of 2 mg/kg and oral administration (PO) of 20 mg/kg to male Sprague Dawley rats are shown in Table 8 and Figure S1. Following a single IV dosing administration, **6b** showed a $t_{1/2}$ of 2.9 h. Systemic clearance was 4.39 L/h/kg, and Vss was 4.59 L/kg. Following a single administration of **6b** PO, the median T_{max} and $t_{1/2}$ were 0.25 h and 16.4 h, respectively. The oral bioavailability (F) was 17.8% based on the $AUC_{0-\infty}$ ratio and was 15.1% based on the AUC_{0-t} ratio.

To determine the *in vitro* metabolism among different species, the metabolic stability of compound **6b** was tested in mouse, rat, dog and human hepatocytes (Fig. 7). The apparent half-life of

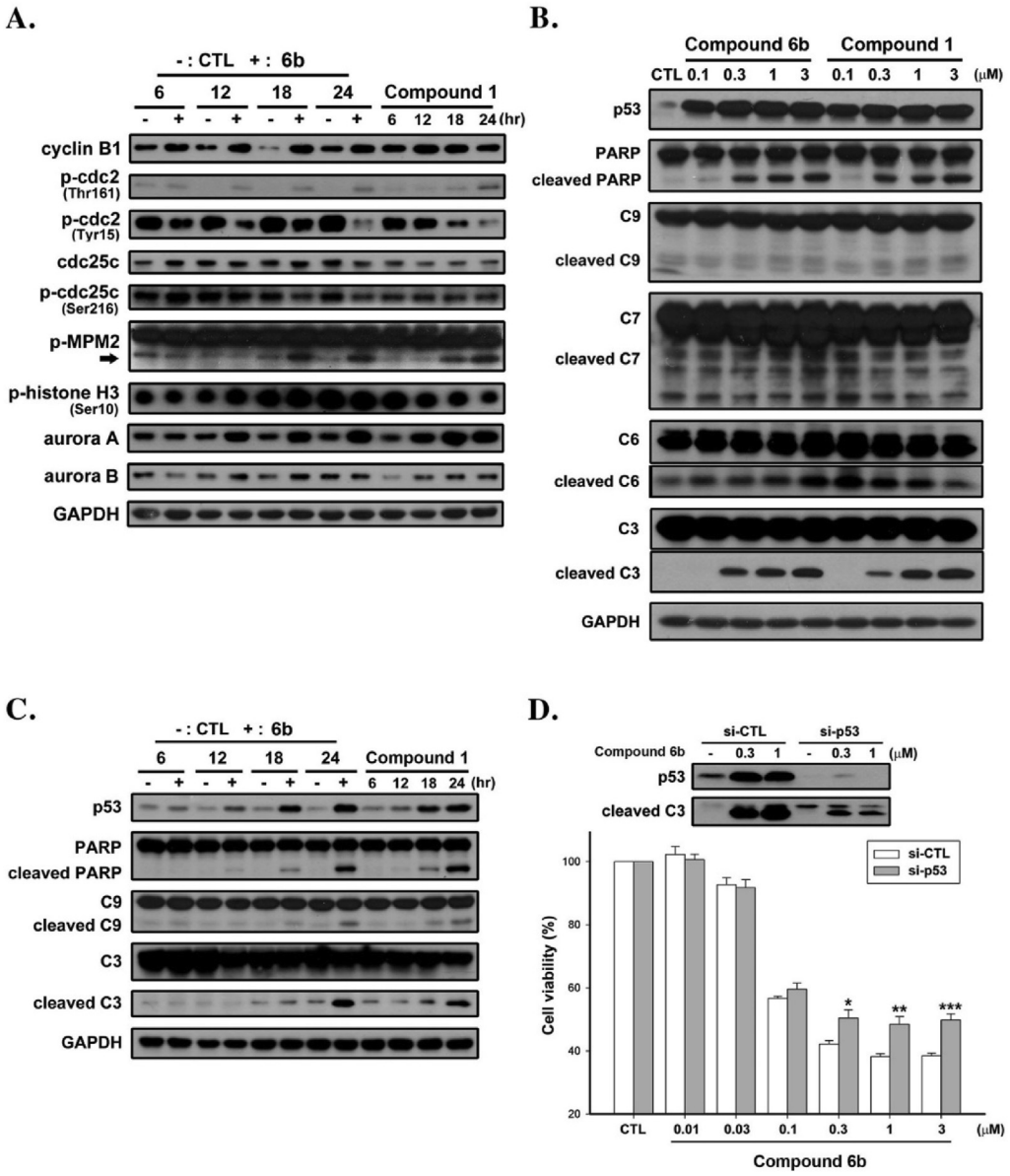

Fig. 6. Effect of compound **6b** on cell cycle progression and apoptotic pathways in human A549 lung cancer cell line. (A) Cells were treated with vehicle (DMSO) or 0.3 μM of indicated drugs for indicated times. After treatment, whole cell lysates were collected and subjected to western blot analysis for the detection of cell cycle-related protein expression. (B) Concentration-dependent and (C) time-dependent effects of compound **6b**-induced p53 accumulation, PARP cleavage, and caspase activation. (D) A549 cells were transfected with si-RNA specific to p53 or scrambled prior to treatment of compound **6b**. After then, western blot was conducted for the detection of p53 and cleaved C3 protein levels, and 48 h MTT assay was performed to measure A549 cell viability. *$p < 0.05$, **$p < 0.01$, and ***$p < 0.001$ as compared with the control group.

Table 4
The cytotoxic effects of compound **6b** and HSP90 inhibitors in 661W by MTT assay.

Compounds	**6b**	**1** (17-AAG)	**2** (BIIB021)	**3a** (AUY922)	**3b** (STA-9090)	Geldanamycin
IC_{50} (μM)[a]	>10	>10	>10	0.04 ± 0.00	>10	1.65 ± 0.6

[a] SD: standard deviation, all experiments were independently performed at least three times.

Table 5
The potassium channel hERG test of compound **6b**.

Compound	Concentration (μM)	Inhibition (%)[a]
6b	10	−18

[a] Potassium channel hERG test was examined by the Eurofin Cerep Panlabs.

compound **6b** in mouse, rat, dog and human hepatocytes was 5.31, 11.22, 39.24, and 67.59 min, respectively (Table 9). The intrinsic clearance ($CL_{int,app}$) and predicted hepatic clearance (CL_{hep}) of compound **6b** were 185.00 and 5.25 L/h/kg in mouse hepatocytes, 45.03 and 3.07 L/h/kg in rat hepatocytes, 7.15 and 1.50 L/h/kg in dog hepatocytes, and 3.32 and 0.88 L/h/kg in human hepatocytes,

Table 6
Direct inhibitory effects (IC_{50} values) of compound **6b** on seven human CYP450 enzymes in pooled human liver microsomes.

CYP enzyme	Substrate	IC_{50} (μM)[a]
CYP1A2	Phenacetin	>50 (50.6%)
CYP2B6	Bupropion	37.17
CYP2C8	Amodiaquine	>50 (54.3%)
CYP2C9	Diclofenac	14.97
CYP2C19	S-Mephenytoin	7.80
CYP2D6	Dextromethorphan	>50 (84.0%)
CYP3A4	Midazolam	3.23
CYP3A4	Testosterone	1.15

[a] When IC_{50} was greater than 50 μM, the percent inhibition value at 50 μM was included (in parentheses); The studies were performed by Development Center for Biotechnology Taiwan.

Table 8
Evaluation of pharmacokinetics parameters in rat.[a].

Parameter	IV (2 mg/kg)	PO (20 mg/kg)	F (%)
T_{max} (h)[b]	0.03 (0.02–0.03)	0.25 (0.25–6.0)	NA
C_{max} (ng/mL)	1580 ± 135	40.5 ± 10.8	NA
$AUC_{(0\text{-}t)}$ (ng mL^{-1} h)	487 ± 32	737 ± 127	15.1[c]
$AUC_{0\text{-}\infty}$ (ng mL^{-1} h)	456	811 ± 164	17.8[d]
$t_{1/2}$ (hr)	2.9	16.4 (14.0–17.4)	NA
V_{ss} (L/kg)	4.59	NA	NA
CL (L/L/kg)	4.39	NA	NA

[a] The studies were performed by QPS Taiwan.
[b] Median (range).
[c] F(%) was calculated as $(AUC_{0\text{-}t,\ PO}/Dose_{PO})/(AUC_{0\text{-}t,\ IV}/Dose_{IV})$.
[d] F(%) was calculated as $(AUC_{0\text{-}\infty,\ PO}/Dose_{PO})/(AUC_{0\text{-}\infty,\ IV}/Dose_{IV})$; NA: Not applicable.

respectively. In addition, compound **6b** showed a high hepatic extraction ratio in mouse (E = 0.97) and rat (E = 0.93) hepatocytes, and moderate to high hepatic extraction ratio in dog (E = 0.79) and human (E = 0.73) hepatocytes. This indicates that **6b** is likely to be cleared rapidly through the liver.

*2.2.11. In vivo antitumor efficacy of compound **6b** in human A549 lung cancer xenografts*

Based on a few significant outcomes of HSP90 inhibitors used in NSCLC treatment that have been reported recently, compound **6b** was evaluated for *in vivo* efficacy against tumor xenografts in human A549 lung cancer xenografts (n = 7) (Fig. 8). Compound **6b** displayed antitumor activity at doses of 25 mg/kg and 50 mg/kg, suppressing the growth with 46.7% (*$p < 0.05$) and 46.9% (*$p < 0.05$) of TGI (tumor growth inhibition) after oral administration, respectively (Fig. 8A). No significant differences in weight loss were observed during all the treatments (Fig. 8B). Moreover, compound **6b** significant enhanced tumor growth delay (TGD, 72%) compared to a vehicle treated group. (Fig. 8C) (Table 10).

*2.2.12. In vivo antitumor efficacy of compound **6b** in human H1975 lung cancer xenografts*

The antitumor efficacy of compound **6b** in human H1975 lung cancer xenograft was evaluated employing afatinib and STA-9090 (**3b**) as reference compounds (Fig. 9). Compound **6b** has shown antitumor activity and reduction in tumor volume at 50 mg/kg with TGI as 34.3% (**$p < 0.01$) without any significant body weight loss during the treatment period (Fig. 9A and B, n = 8). The effect of afatinib, STA-9090, and compound **6b** in combination was examined as shown in Fig. 9C and D (n = 9). The combination therapy led to substantially higher reductions in the tumor volume. Monotherapy with **6b** resulted in TGI of 25.5% (***$p < 0.001$) at 200 mg/kg (po, q3d) and 27.2% (***$p < 0.001$) at 50 mg/kg (po, qd). While compound **6b** at doses of 200 mg/kg (po, q3d) and 50 mg/kg (po, qd) in combination with afatinib (25 mg/kg, po, qd), resulted in suppressing tumor growth by a TGI of 50.5% (***$p < 0.001$) and 67.5% (***$p < 0.001$), respectively, without considerable body

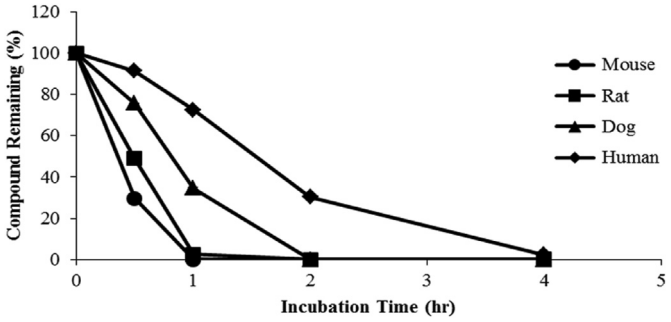

Fig. 7. Time course of stability in mouse, rat, dog and human hepatocytes.

weight loss (Fig. 9C and D). Compound **6b** combined with afatinib showed synergistic antitumor effect compared to the single treatment. Compound **3b** (150 mg/kg, iv, once weekly) [17] single or combined with afatinib, did not exhibit antitumor activity ($p > 0.05$) but was associated with treatment-related animal death in monotherapy (4/9 dead) or combination therapy (8/9 dead). Compared with reference compound **3b**, compound **6b** seems to be a safer and more efficacious HSP90 inhibitor.

3. Conclusion

We have synthesized a series of ring-opened dihydroxybenzamide compounds (**6a-6d**, **7a-7d**, and **8a-8i**). Among all these synthetic compounds, compound **6b** was observed to be a HSP90 inhibitor with an HSP90α inhibitory IC_{50} of 110.18 nM, which is slightly better than reference compound **1**. It can efficiently inhibit the migration of A549 cells compared to the reference compound **1**. Compound **6b** also has substantial *in vitro* antiproliferative activity and *in vivo* antitumor activity. Our results show that **6b** exhibits significant inhibitory activity in human KRAS mutant A549, EGFR T790 M mutant H1975, HCT116 and MDA-MB-231 with IC_{50} values of 70, 50, 90 and 90 nM, respectively, and shows no evidence of

Table 7
Permeability and efflux ratio of compound **6b** and reference compounds in both directions across Caco-2 cell monolayers.

Compound	**6b**	Verapamil	Atenolol	Rhodamine 123
P_{app} (A to B)[a] (x 10^{-6} cm/s)	31.86 ± 5.12	14.39 ± 1.11	0.45 ± 0.06	0.53 ± 0.68
P_{app} (B to A)[a] (x 10^{-6} cm/s)	30.60 ± 2.14	–	–	8.04 ± 1.68
Assay acceptance criteria (cm/sec)	$P_{app} \geq 10 \times 10^{-6}$	$P_{app} \geq 10 \times 10^{-6}$	$P_{app} < 5 \times 10^{-6}$	–
Efflux ratio	0.96	–	–	15.17
Classification	High permeable	High permeable	Low permeable	Substrate of efflux transporter

[a] Permeability coefficient (P_{app}) for apical to basolateral (A to B); The studies were performed by Development Center for Biotechnology Taiwan.

Table 9
Hepatocytes stability of compound 6 in mouse, rat, dog and human.[a].

Compound	Species Hepatocytes	$T_{1/2}$ (min)	CL_{int} (L/h/kg)	CL_{hep} (L/h/kg)	Extraction ratio	Clearance classification
6b	Mouse	5.31	185.00	5.25	0.97	High
	Rat	11.22	45.03	3.07	0.93	High
	Dog	39.24	7.15	1.50	0.79	Moderate to High
	Human	67.59	3.32	0.88	0.73	Moderate to High

[a] The studies were performed by QPS Taiwan.

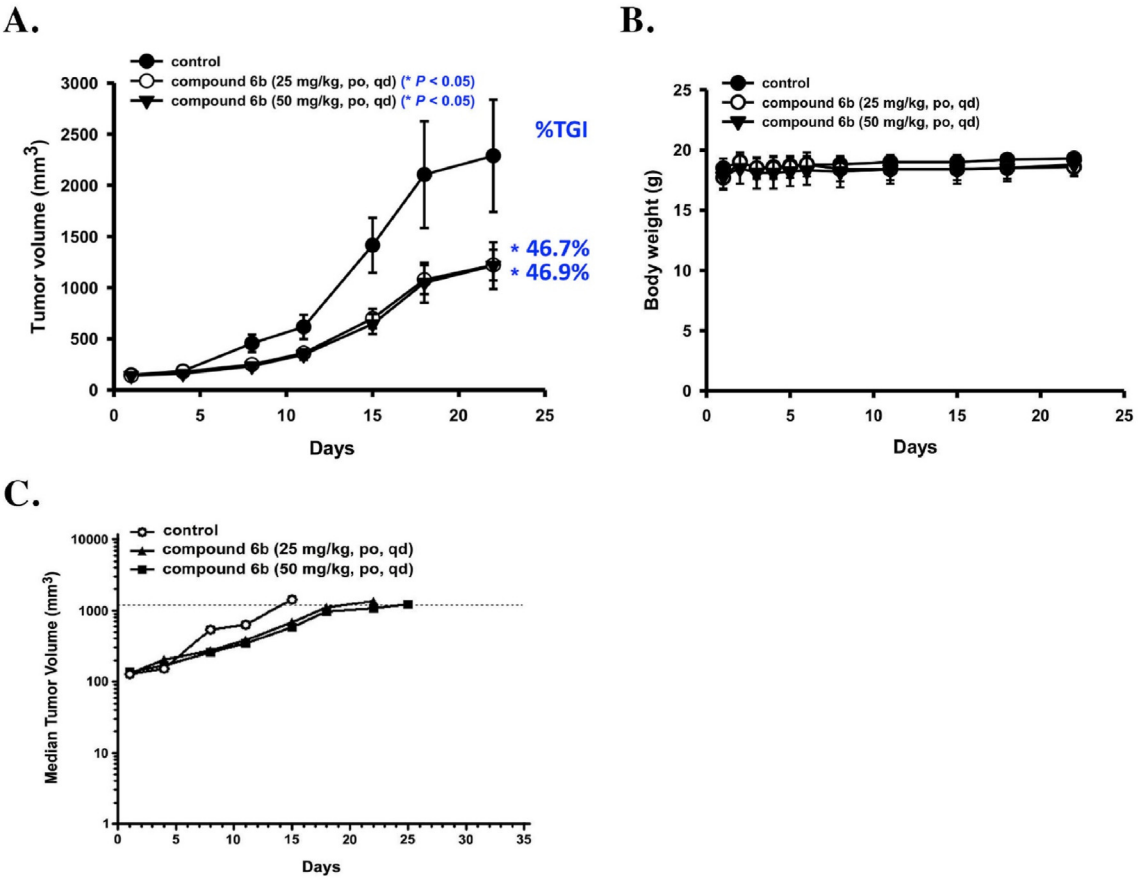

Fig. 8. In vivo antitumor efficacy of compound **6b** on human A549 lung xenograft. (A) 1×10^7 A549 cells were injected into 8 wk-old Balb/c nude mice. The mice were divided into three groups (each group n = 7) and treated with vehicle, compound **6b** 25 mg/kg and 50 mg/kg by daily oral administration route. Tumor growth is tracked by the mean tumor volume (mm^3) ± SE and calculated as % tumor growth inhibition (%TGI). (B) Body weight change after drug treatment. (C) Tumor growth delay (TGD) induced by compound **6b** in A549 xenograft. *p < 0.05, **p < 0.01, and ***p < 0.001 as compared with the control group.

toxicity in normal cell line. Compound **6b** inhibits tumor growth by 46.9% and has a tumor growth delay of 72% at 50 mg/kg (po, qd) in human A549 lung xenografts. It has a TGI of 27.2% at 50 mg/kg (po, qd) in a lung H1975 xenograft model. Combination therapy of **6b** at dose of 50 mg/kg (po, qd) and afatinib led to substantially higher reductions in the tumor volume and 67.5% TGI. Combined with afatinib, compound **6b** showed a synergistic antitumor effect compared to treatment with **6b** alone. No significant differences in weight loss were observed during all the treatments. Treatment with **6b** exhibited no vision toxicity on 661w photoreceptor and without effect in hERG test. From the results of the pharmacokinetic study in rats, **6b** shows an oral bioavailability (F) of 17.8%. In a Caco-2 permeability assay, it was indicated that compound **6b** could be classified as a highly permeable compound and might not be a substrate of efflux transporters. In the metabolic stability assay, the half-life and the intrinsic clearance of compound **6b** were 67.59 min and 3.32 L/h/kg in human hepatocytes. The CYP inhibitory potential of **6b** on CYP1A2, 2B6, 2C8, 2C9, 2C19, 2D6 and 3A4 in pooled human liver microsomes was evaluated and CYP3A4 was found to be the most sensitive to **6b**. In conclusion, our study offers evidence for the efficacy and safety of compound **6b**, and reveals its potential as an anti-lung cancer agent.

Table 10
Tumor growth delay by compound **6b** in human A549 lung xenograft.

Treatment	Dose (mg/kg)	Median TTE[a]	T-C[b]	TGD (%)[c]
Control	–	13.8	–	–
Compound **6b**	25	19.5	5.7	41
Compound **6b**	50	23.8	10	72

[a] TTE: time to endpoint.
[b] T-C: difference between median TTE of treated vs control group.
[c] % TGD (Tumor growth delay): [(T-C)/C] x 100.

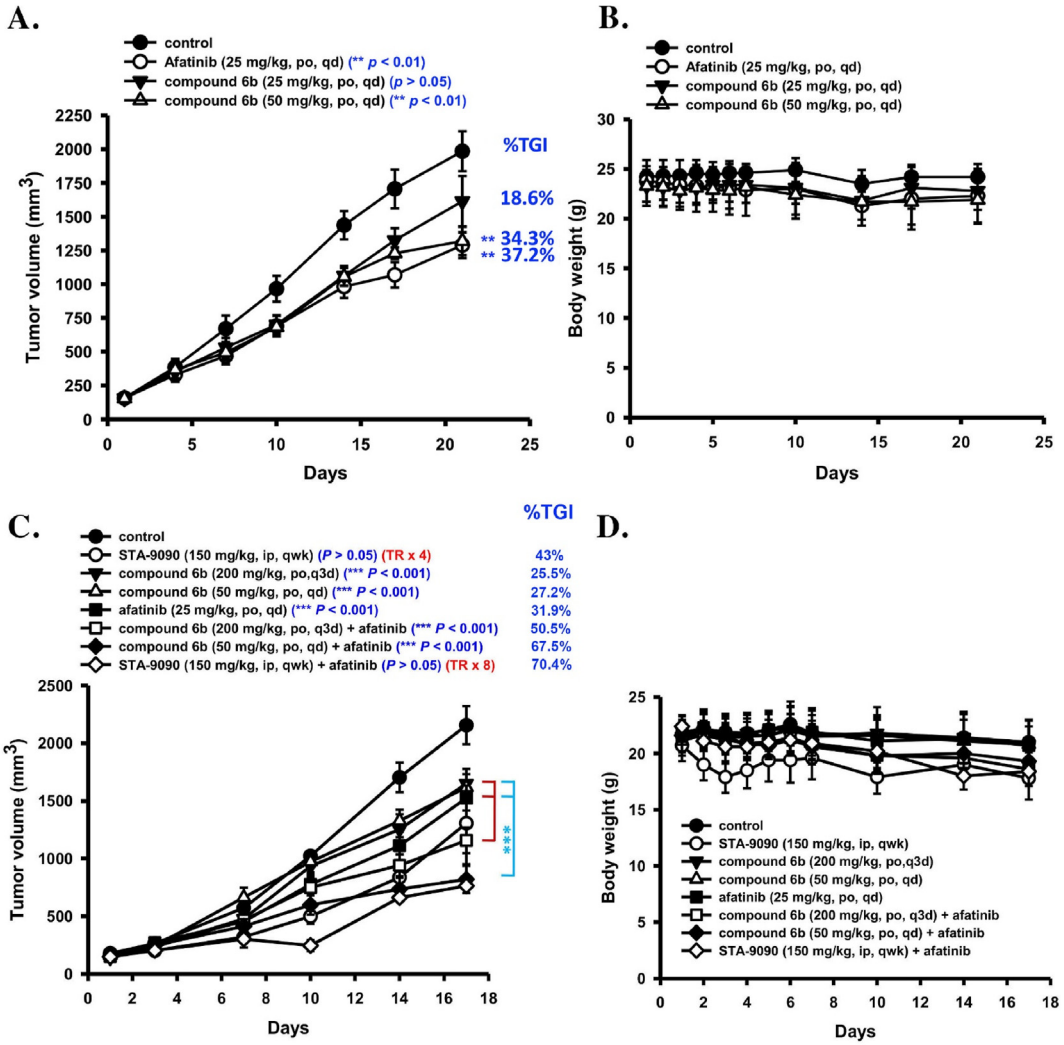

Fig. 9. Anticancer activities of HSP90 inhibitors and afatinib in human lung cancer H1975 xenograft models. (A) 1×10^7 H1975 cells were injected into 8 wk-old Balb/c nude mice. The mice were divided into four groups (each group n = 9) and treated with vehicle, afatinib 25 mg/kg, compound **6b** 25 mg/kg and 50 mg/kg by daily oral administration route. Tumor growth is tracked by the mean tumor volume (mm^3) ± SE and calculated as % tumor growth inhibition (%TGI). (B) Body weight change after treatment. (C) The effect of compound **6b**, afatinib and STA-9090 alone or in combination treatment. (each group n = 9) (D) Body weight change after treatment. *p < 0.05, **p < 0.01, and ***p < 0.001 as compared with the control group. TR, treatment related death.

4. Experimental section

4.1. Chemistry

Nuclear magnetic resonance (^{1}H and ^{13}CNMR) spectra were obtained with a Bruker DRX-500 spectrometer operating at 500 or 125 MHz. Chemical shifts are reported in parts per million (ppm, δ) downfield from TMS as an internal standard. Low-resolution mass spectra (LRMS) were measured with TSQ-700 (Finnigan, Germany). High-resolution mass spectra (HRMS) were measured with a JEOL (JMS-700) electron impact (EI) mass spectrometer. The purities of the final compounds were determined using a Waters Acquity UPLC/BSM with PhotoDiode Array detector using C-18 column (Waters Acquity BEH-C18, 2.1 mm (ID) x 50 mm (L), 1.7 μm particle size) with the solvent system consisting of water containing 0.1% formic acid + 2 mM NH_4OAc (mobile phase A) and acetonitrile (mobile phase B), and were found to be ≧ 95%. Flash column chromatography was accomplished on silica gel (Merck Kieselgel 60, No. 9385, 230–400 mesh ASTM). All reactions were carried out under an atmosphere of dry nitrogen.

4.1.1. Syntheses of compound *6-8*

*4.1.1.1. 2,4-Dihydroxy-5-isopropyl-N-(pyridin-3-yl)benzamide (**6a**).* A mixture of **10** (0.42 g, 0.93 mmol), 10% palladium on activated carbon (0.04 g, 0.04 mmol) and MeOH (8 ml) was placed under hydrogen gas. The reaction was stirred at room temperature for 2 h. The 10% palladium on activated carbon was removed by a methyl alcohol wash through celite packing. The organic layer was concentrated *in vacuo* and purified by silica gel chromatography (EtOAc:n-hexane = 2: 1, Rf = 0.3) to afford **6a** (0.22 g, 88.0%) as a white solid. m.p. 269.1–270.3 °C. ^{1}H NMR (500 MHz, MeOD): δ 1.24 (d, J = 7 Hz, 6H), 3.20 (Sep, J = 7 Hz, 1H), 6.35 (s, 1H), 7.41–7.43 (m, 1H), 7.75 (s, 1H), 8.17–8.20 (m, 1H), 8.27–8.28 (m, 1H), 8.82 (d, J = 2.5 Hz, 1H). ^{13}C NMR (125 MHz, DMSO-d_6): δ 22.64, 26.15, 102.59, 107.23, 123.55, 126.58, 126.66, 128.50, 134.99, 142.82, 144.80, 159.03, 159.99, 167.54. hMS (ESI) for $C_{15}H_{15}N_2O_3$ [M − H]$^-$: calcd, 271.1088; found, 271.1081.

*4.1.1.2. N-Ethyl-2,4-dihydroxy-5-isopropyl-N-(pyridin-3-yl)benzamide (**6b**).* A mixture of **10** (0.35 g, 0.77 mmol), NaH (0.04 g, 1.0 mmol) and DMF (4 ml) was added to ethyl iodide (0.1 ml,

1.24 mmol) at R.T. for 2 h. The reaction was quenched with water and extracted with EtOAc (30 ml x 3). The organic layer was collected and dried over anhydrous $MgSO_4$ concentrated *in vacuo* and purified by silica gel chromatography (EtOAc:n-hexane = 2: 1, Rf = 0.4) to get the oily product, then the oily product was dissolved in MeOH (8 ml) and added 10% palladium on activated carbon (0.04 g, 0.04 mmol) under the hydrogen gas. The reaction was stirred at R.T. for 2 h. The 10% palladium on activated carbon was removed by methyl alcohol washed through celite packing. The organic layer was concentrated *in vacuo* and purified by silica gel chromatography (EtOAc:n-hexane = 2: 1, Rf = 0.3) to afford **6b** (0.16 g, 69.57%) as a yellow solid. m.p. 179.6–181.5 °C. ^{1}H NMR (500 MHz, MeOD): δ 0.90 (d, J = 7 Hz, 6H), 1.20 (t, J = 7 Hz 3H), 2.96 (Sep, J = 7 Hz, 1H), 3.95 (q, J = 7 Hz, 2H), 6.15 (s, 1H), 6.66 (s, 1H), 7.38–7.41 (m, 1H), 7.69–7.71 (m, 1H), 8.28 (d, J = 2 Hz, 1H), 8.33–8.34 (m, 1H). ^{13}C NMR (125 MHz, MeOD): δ 13.26, 23.08, 27.18, 46.48, 103.47, 112.03, 125.60, 127.68, 128.91, 137.08, 142.36, 147.93, 149.64, 157.95, 159.54, 172.97. hMS (ESI) for $C_{17}H_{20}N_2NaO_3$ $[M+Na]^+$: calcd, 323.1366; found, 323.1357.

*4.1.1.3. 2,4-Dihydroxy-5-isopropyl-N-propyl-N-(pyridin-3-yl)benzamide (**6c**).* The synthetic procedure for compound **6c** is similar to that used for compound **6b** and gave a yield of 67.85% as a white solid. m.p. 196.3–198.2 °C. ^{1}H NMR (500 MHz, MeOD): δ 0.92 (m, 9H), 1.63 (6, J = 7.5 Hz, 2H), 2.97 (Sep, J = 7 Hz, 1H), 3.87 (t, J = 7.5 Hz, 2H), 6.14 (s, 1H), 6.66 (s, 1H), 7.37–7.41 (m, 1H), 7.69–7.71 (m, 1H), 8.28–8.32 (m, 2H). ^{13}C NMR (125 MHz, MeOD): δ 11.69, 22.14, 23.10, 27.21, 52.97, 103.47, 112.38, 125.56, 127.72, 128.82, 136.95, 142.60, 147.85, 149.54, 157.67, 159.46, 173.18. hMS (ESI) for $C_{18}H_{22}N_2NaO_3$ $[M+Na]^+$: calcd, 337.1523; found, 337.1516.

*4.1.1.4. 2,4-Dihydroxy-N,5-diisopropyl-N-(pyridin-3-yl)benzamide (**6d**).* The synthetic procedure for compound **6d** is similar to that used for compound **6b** and gave a yield of 60.25% as a yellow solid. m.p. 172.4–174.3 °C. ^{1}H NMR (500 MHz, MeOD): δ 0.96 (d, J = 6.5 Hz, 6H), 1.19 (d, J = 7 Hz, 6H), 2.98 (Sep, J = 7 Hz, 1H), 4.96 (Sep, J = 7 Hz, 1H), 6.11 (s, 1H), 6.66 (s, 1H), 7.36–7.39 (m, 1H), 7.67–7.69 (m, 1H), 8.29 (d, J = 2.5 Hz, 1H), 8.36–8.37 (m, 1H). ^{13}C NMR (125 MHz, MeOD): δ 21.48, 23.18, 27.28, 49.84, 103.36, 114.37, 125.15, 127.61, 127.99, 138.58, 139.93, 148.82, 151.68, 156.24, 158.64, 173.26. hMS (ESI) for $C_{18}H_{22}N_2NaO_3$ $[M+Na]^+$: calcd, 337.1523; found, 337.1517.

*4.1.1.5. 2,4-Dihydroxy-5-isopropyl-N-(pyridin-4-yl)benzamide (**7a**).* The synthetic procedure for compound **7a** is similar to that used for compound **6a** and gave a yield of 86.95% as a yellow solid. m.p. 235.9–238.3 °C. ^{1}H NMR (500 MHz, MeOD): δ 1.23 (d, J = 7 Hz, 6H), 3.19 (Sep, J = 7 Hz, 1H), 6.36 (s, 1H), 7.76–7.77 (m, 3H), 8.40 (d, J = 6.5 Hz, 2H). ^{13}C NMR (125 MHz, MeOD): δ 23.14, 28.17, 103.84, 109.12, 116.18, 128.31, 129.24, 148.40, 150.73, 160.85, 162.36, 169.99. hMS (ESI) for $C_{15}H_{17}N_2O_3$ $[M+H]^+$: calcd, 273.1234; found, 273.1240.

*4.1.1.6. N-Ethyl-2,4-dihydroxy-5-isopropyl-N-(pyridin-4-yl)benzamide (**7b**).* The synthetic procedure for compound **7b** is similar to that used for compound **6b** and gave a yield of 63.64% as a white solid. m.p. 185.2–186.1 °C. ^{1}H NMR (500 MHz, MeOD): δ 0.86 (d, J = 7 Hz, 6H), 1.21 (t, J = 7 Hz, 3H), 2.97 (Sep, J = 7 Hz, 1H) 4.01 (q, J = 7 Hz, 2H), 6.20 (s, 1H), 6.68 (s, 1H), 7.17–7.18 (m, 2H), 8.39–8.41 (m, 2H). ^{13}C NMR (125 MHz, MeOD): δ 13.53, 22.93, 27.07, 45.98, 103.58, 110.91, 123.09, 127.81, 129.57, 151.14, 154.14, 159.34, 160.44, 173.25. hMS (ESI) for $C_{17}H_{20}N_2NaO_3$ $[M+Na]^+$: calcd, 323.1366; found, 323.1360.

*4.1.1.7. 2,4-Dihydroxy-5-isopropyl-N-propyl-N-(pyridin-4-yl)benzamide (**7c**).* The synthetic procedure for compound **7c** is similar to that used for compound **6b** and gave a yield of 63.64% as a white solid. m.p. 196.3–198.2 °C. ^{1}H NMR (500 MHz, MeOD): δ 0.86 (d, J = 7 Hz, 6H), 0.94 (t, J = 7.5 Hz, 3H), 1.65 (Sex, J = 7.5 Hz, 2H), 2.97 (Sep, J = 7 Hz, 1H), 3.92 (t, J = 7.5 Hz, 2H), 6.20 (s, 1H), 6.68 (s, 1H), 7.17–7.18 (m, 2H), 8.38–8.39 (m, 2H). ^{13}C NMR (125 MHz, MeOD): δ 11.67, 22.36, 22.93, 27.06, 52.35, 103.55, 111.09, 122.95, 127.81, 129.51, 151.07, 154.35, 159.16, 160.36, 173.42. hMS (ESI) for $C_{18}H_{22}N_2NaO_3$ $[M+Na]^+$: calcd, 337.1523; found, 337.1514.

*4.1.1.8. 2,4-Dihydroxy-N,5-diisopropyl-N-(pyridin-4-yl)benzamide (**7d**).* The synthetic procedure for compound **7d** is similar to that used for compound **6b** and gave a yield of 60.25% as a white solid. m.p. 165.4–166.6 °C. ^{1}H NMR (500 MHz, MeOD): δ 0.89 (d, J = 7 Hz, 6H), 1.27 (d, J = 6.5 Hz, 6H), 2.96 (Sep, J = 7 Hz, 1H), 4.89 (Sep, J = 7 Hz, 1H), 6.15 (s, 1H), 6.63 (s, 1H), 7.21 (d, J = 6 Hz, 2H), 8.43–8.45 (m, 2H). ^{13}C NMR (125 MHz, MeOD): δ 21.38, 23.02, 27.11, 51.03, 103.40, 112.91, 126.41, 127.54, 128.66, 150.98, 151.43, 157.95, 159.35, 173.09. hMS (ESI) for $C_{18}H_{22}N_2NaO_3$ $[M+Na]^+$: calcd, 337.1523; found, 337.1513.

*4.1.1.9. 2,4-Dihydroxy-N-(1H-indol-5-yl)-5-isopropylbenzamide (**8a**).* A mixture of **13** (0.5 g, 0.85 mmol) was dissolved in DCM (5 ml) and added TFA (1 ml) at R.T. for 2 h. The reaction was quenched with water and extracted with EtOAc (30 ml x 3). The organic layer was collected and dried over anhydrous $MgSO_4$ concentrated *in vacuo* and without further purification. The crude product was dissolved in MeOH (8 ml) and added 10% palladium on activated carbon (0.04 g, 0.04 mmol) under the hydrogen gas. The reaction was stirred at R.T. for 2 h. The 10% palladium on activated carbon was removed by a methyl alcohol wash through celite packing. The organic layer was concentrated *in vacuo* and purified by silica gel chromatography (EtOAc:n-hexane = 1: 1, Rf = 0.4) to afford **8a** (0.19 g, 73.07%) as a green solid. m.p. 221.1–223.7. ^{1}H NMR (500 MHz, MeOD): δ 1.22 (d, J = 6.5 Hz, 6H), 3.19 (Sep, J = 7 Hz, 1H), 6.35 (s, 1H), 6.41 (d, J = 7 Hz, 1H), 7.15 (d, J = 2 Hz, 1H), 7.15–7.22 (m, 1H), 7.32 (d, J = 8.5 Hz, 1H), 7.70–7.73 (m, 2H). ^{13}C NMR (125 MHz, MeOD): δ 23.20, 28.11, 102.66, 103.79, 109.12, 112.22, 115.85, 118.99, 126.64, 127.37, 128.67, 129.63, 130.76, 135.63, 160.99, 161.33, 170.16. hMS (ESI) for $C_{18}H_{18}N_2NaO_3$ $[M+Na]^+$: calcd, 333.1210; found, 333.1212.

*4.1.1.10. 2,4-Dihydroxy-N-(1H-indol-5-yl)-5-isopropyl-N-methylbenzamide (**8b**).* A mixture of **13** (0.8 g, 1.35 mmol), NaH (0.07 g, 1.75 mmol) and DMF (5 ml) was added to methyl iodide (0.2 ml, 3.22 mmol) at R.T. for 2 h. The reaction was quenched with water and extracted with EtOAc (30 ml x 3). The organic layer was collected and dried over anhydrous $MgSO_4$ concentrated *in vacuo* and purified by silica gel chromatography (EtOAc:n-hexane = 1: 2, Rf = 0.6) to get the oily product. This was then dissolved in DCM (5 ml) and added TFA (1 ml) at R.T. for 2 h. The reaction was quenched with water and extracted with EtOAc (30 ml x 3). The organic layer was collected and dried over anhydrous $MgSO_4$ concentrated *in vacuo* and without more purification. The crude product was dissolved in MeOH (8 ml), THF (8 ml) and added to 10% palladium on activated carbon (0.04 g, 0.04 mmol) under hydrogen gas and 40 psi at R.T. for overnight. The 10% palladium on activated carbon was removed by a methyl alcohol wash through celite packing. The organic layer was concentrated *in vacuo* and purified by silica gel chromatography (EtOAc:n-hexane = 1: 2, Rf = 0.55) to afford **8b** (0.25 g, 56.82%)as a white solid. m.p. 217.7–219.5. ^{1}H NMR (500 MHz, MeOD): δ 0.49 (d, J = 7 Hz, 6H), 2.74 (qui, J = 7 Hz, 1H), 3.46 (s, 3H), 6.16 (s, 1H), 6.41 (d, J = 3 Hz, 1H), 6.48 (s, 1H), 6.93–6.95 (m, 1H), 7.26 (d, J = 3 Hz, 1H), 7.33 (s, 1H), 7.37 (d, J = 8.5 Hz, 1H). ^{13}C

NMR (125 MHz, MeOD): δ 22.69, 26.73, 40.30, 102.95, 103.29, 113.34, 119.66, 121.33, 126.72, 127.40, 130.00, 130.22, 136.61, 138.85, 159.45, 173.50. hMS (ESI) for $C_{19}H_{20}N_2NaO_3$ $[M+Na]^+$: calcd, 347.1366; found, 347.1365.

*4.1.1.11. N-Ethyl-2,4-dihydroxy-N-(1H-indol-5-yl)-5-isopropylbenzamide (**8c**).* The synthetic procedure for compound **8c** is similar to that used for compound **8b** and gave a yield of 51.16% as a white solid. m.p. 234.4–236.7 °C. ^{1}H NMR (500 MHz, MeOD): δ 0.46 (d, *J* = 6.5 Hz, 6H), 1.21 (t, *J* = 7 Hz, 3H), 2.72 (Sex, *J* = 7 Hz, 1H), 3.94 (q, *J* = 7 Hz, 2H), 6.17 (s. 1H), 6.39 (d, *J* = 3 Hz, 1H), 6.45 (s, 1H), 6.90–6.92 (m, 1H), 7.24 (d, *J* = 3 Hz, 1H), 7.30 (d, *J* = 2 Hz, 1H), 7.37 (d, *J* = 8.5 Hz, 1H). ^{13}C NMR (125 MHz, MeOD): δ 13.03, 22.70, 26.73, 47.67, 102.94, 103.27, 113.25, 120.69, 122.23, 126.65, 127.35, 129.94, 130.19, 136.68, 136.80, 159.33, 172.96. hMS (ESI) for $C_{20}H_{22}N_2NaO_3$ $[M+Na]^+$: calcd, 361.1523; found, 361.1524.

*4.1.1.12. 2,4-Dihydroxy-N-(1H-indol-5-yl)-5-isopropyl-N-propylbenzamide (**8d**).* The synthetic procedure for compound **8d** is similar to that used for compound **8b** and gave a yield of 51.06% as a white solid. m.p. 206.0–207.8 °C. ^{1}H NMR (500 MHz, MeOD): δ 0.48 (d, *J* = 6.5 Hz, 6H), 0.93 (t, *J* = 7.5 Hz, 3H), 1.66 (Sex, *J* = 7.5 Hz, 2H), 2.73 (Sex, *J* = 6.5 HZ, 1H), 3.86 (t, *J* = 7.5 Hz, 2H), 6.16 (s, 1H), 6.40 (d, *J* = 3 Hz, 1H), 6.46 (s, 1H), 6.91 (s, 1H), 7.25 (d, *J* = 3.5 Hz, 1H), 7.31 (d, *J* = 1.5 Hz, 1H), 7.34 (d, *J* = 8.5 Hz, 1H). ^{13}C NMR (125 MHz, MeOD): δ 11.81, 21.77, 22.68, 26.71, 54.31, 102.91, 103.25, 113.18, 120.51, 122.10, 126.62, 127.33, 129.82, 130.14, 136.62, 137.01, 159.23, 173.11. hMS (ESI) for $C_{21}H_{24}N_2NaO_3$ $[M+Na]^+$: calcd, 375.1679; found, 375.1676.

*4.1.1.13. 2,4-Dihydroxy-N-(1H-indol-5-yl)-N,5-diisopropylbenzamide (**8e**).* The synthetic procedure for compound **8e** is similar to that used for compound **8b** and gave a yield of 47.91% as a white solid. m.p. 226.1–227.9 °C. ^{1}H NMR (500 MHz, MeOD): δ 0.56 (d, *J* = 5.5 Hz, 6H), 1.19 (d, *J* = 7 Hz, 6H), 2.76 (qui, *J* = 7 Hz, 1H), 5.04 (t, *J* = 5.5 Hz, 1H), 6.13 (s, 1H), 6.42 (d, *J* = 3 Hz, 1H), 6.49 (s, 1H), 6.85–6.88 (m, 1H), 7.24 (d, *J* = 3 Hz, 1H), 7.31 (d, *J* = 1.5 Hz, 1H), 7.33 (d, *J* = 9 Hz, 1H). ^{13}C NMR (125 MHz, MeOD): δ 21.43, 22.77, 26.76, 102.93, 103.20, 112.46, 122.92, 124.60, 126.53, 127.11, 129.17, 129.73, 136.87, 158.58, 173.25. hMS (ESI) for $C_{21}H_{24}N_2NaO_3$ $[M+Na]^+$: calcd, 375.1679; found, 375.1681.

*4.1.1.14. 2,4-Dihydroxy-5-isopropyl-N-(1-methyl-1H-indol-5-yl)benzamide (**8f**).* The synthetic procedure for compound **8f** is similar to that used for compound **6a** and gave a yield of 47.91% as a pink solid. m.p. 221.2–223.8 °C. ^{1}H NMR (500 MHz, MeOD): δ 1.25 (d, *J* = 7 Hz, 6H), 3.21 (Sep, *J* = 7 Hz, 1H), 3.75 (s, 1H), 6.35 (s, 1H), 6.39 (d, *J* = 3 Hz, 1H), 7.11 (d, *J* = 3 Hz, 1H), 7.26–7.28 (m, 1H), 7.31 (d, *J* = 8.5 Hz, 1H), 7.74 (d, *J* = 1.5 Hz, 1H), 7.77 (s, 1H). ^{13}C NMR (125 MHz, MeOD): δ 23.22, 28.13, 33.08, 101.93, 103.82, 109.15, 110.29, 116.10, 118.95, 127.41, 128.68, 130.18, 131.04, 136.27, 161.03, 161.36, 170.13. hMS (ESI) for $C_{19}H_{20}N_2NaO_3$ $[M+Na]^+$: calcd, 347.1366; found, 347.1370.

*4.1.1.15. 2,4-Dihydroxy-5-isopropyl-N-methyl-N-(1-methyl-1H-indol-5-yl)benzamide (**8g**).* The synthetic procedure for compound **8g** is similar to that used for compound **6b** and gave a yield of 75.0% as a white solid. m.p. 157.2–158.4 °C. ^{1}H NMR (500 MHz, MeOD): δ 0.49 (d, *J* = 6.5 Hz, 6H), 2.74 (qui, *J* = 7 Hz, 1H), 3.46 (s, 3H), 3.78 (s, 3H), 6.15 (s, 1H), 6.39 (d, *J* = 8 Hz, 1H), 6.45 (s, 1H), 6.99–7.01 (m, 1H), 7.18 (d, *J* = 3 Hz, 1H), 7.35 (d, *J* = 5 Hz, 1H), 7.37 (s, 1H). ^{13}C NMR (125 MHz, MeOD): δ 22.73, 26.73, 33.13, 40.20, 102.28, 103.30, 111.41, 120.03, 121.50, 126.73, 129.88, 130.76, 131.79, 137.20, 139.00, 159.41, 173.53. hMS (ESI) for $C_{20}H_{22}N_2NaO_3$ $[M+Na]^+$: calcd, 361.1523; found, 361.1520.

*4.1.1.16. N-Ethyl-2,4-dihydroxy-5-isopropyl-N-(1-methyl-1H-indol-5-yl)benzamide (**8h**).* The synthetic procedure for compound **8h** is similar to that used for compound **6b** and gave a yield of 70.83% as a white solid. m.p. 167.6–169.8 °C. ^{1}H NMR (500 MHz, MeOD): δ 0.47 (d, *J* = 6.5 Hz, 6H), 1.19 (t, *J* = 7 Hz, 3H), 2.73 (Sex, *J* = 7 Hz, 1H), 3.74 (s, 3H), 3.93 (q, *J* = 7 Hz, 2H), 6.17 (s, 1H), 6.37 (d, *J* = 3 Hz, 1H), 6.44 (s, 1H), 6.94–6.96 (m, 1H), 7.15 (d, *J* = 3 Hz, 1H), 7.30–7.33 (m 2H). ^{13}C NMR (125 MHz, MeOD): δ 13.04, 22.73, 26.72, 33.14, 47.59, 102.26, 103.28, 111.32, 121.03, 122.42, 126.65, 129.81, 130.74, 131.74, 136.96, 137.27, 159.30, 172.99. hMS (ESI) for $C_{21}H_{24}N_2NaO_3$ $[M+Na]^+$: calcd, 375.1679; found, 375.1679.

*4.1.1.17. 2,4-Dihydroxy-5-isopropyl-N-(1-methyl-1H-indol-5-yl)-N-propylbenzamide (**8i**).* The synthetic procedure for compound **8i** is similar to that used for compound **6b** and gave a yield of 75.0% as a white solid. m.p. 179.9–182.4 °C. ^{1}H NMR (500 MHz, MeOD): δ 0.49 (d, *J* = 6.5 Hz, 6H), 0.93 (t, *J* = 7 Hz, 3H), 1.66 (Sex, *J* = 7.5 Hz, 2H), 2.73 (Sex, *J* = 7 Hz, 1H), 3.77 (s, 1H), 3.87 (t, *J* = 7.5 Hz, 2H), 6.15 (s, 1H), 6.38 (d, *J* = 2.5 Hz, 1H), 6.43 (s, 1H), 6.96–6.98 (m, 1H), 7.17 (d, *J* = 3 Hz, 1H), 7.32–7.35 (m, 2H). ^{13}C NMR (125 MHz, MeOD): δ 11.81, 21.78, 22.72, 26.70, 33.11, 54.23, 102.23, 103.26, 111.25, 120.84, 122.29, 126.62, 129.69, 130.67, 131.70, 137.20, 159.19, 173.13. hMS (ESI) for $C_{22}H_{26}N_2NaO_3$ $[M+Na]^+$: calcd, 389.1836; found, 389.1833.

*4.1.2. 2,4-bis(Benzyloxy)-5-isopropylbenzoic acid (**9**)*

A mixture of **19** (3 g, 8.32 mmol), sulfamic acid (6.5 g, 66.94 mmol), DMSO (2 ml), THF (20 ml) and water (20 ml) was added to $NaClO_2$ (6 g, 66.34 mmol) dissolved in water (20 ml) at 0 °C. The reaction was allowed back to R.T. and stirred for 2 h. The residue was extracted with EtOAc (40 ml x 3) and purified by silica gel chromatography (EtOAc:n-hexane = 1: 4, Rf = 0.25) to afford **9** (2.02 g, 64.61%) as a yellow solid.^{1}H NMR (500 MHz, $CDCl_3$): δ 1.23 (d, *J* = 7 Hz, 6H), 2.98 (s, 1H), 3.30 (Sep, *J* = 7 Hz, 1H), 5.10 (s, 2H), 5.20 (s, 2H), 6.57 (s, 1H), 7.34–7.44 (m, 10H), 8.03 (s, 1H).

*4.1.3. 2,4-bis(Benzyloxy)-5-isopropyl-N-(pyridin-3-yl)benzamide (**10**)*

A mixture of **9** (2 g, 5.31 mmol), EDC.HCl (1.5 g, 7.85 mmol), HOBt (0.9 g, 6.67 mmol), NMM (1.4 ml, 12.75 mmol) and DMF (8 ml) was stirred for 10 min then 3-aminopyridine (0.6 g, 6.38 mmol) was added at R.T. for overnight, the reaction was quenched with water and extracted with EtOAc (30 ml x 3). The organic layer was collected and dried over anhydrous $MgSO_4$ concentrated *in vacuo* to yield colorless oil product. The residue was purified by silica gel chromatography (EtOAc:n-hexane = 2: 1, Rf = 0.4) to afford **10** (1.76 g, 73.33%) as a white solid. ^{1}H NMR (500 MHz, $CDCl_3$): δ 1.27 (d, *J* = 7.0 Hz, 6H), 3.36 (Sep, *J* = 7.0 Hz, 1H), 5.15 (s, 2H), 5.18 (s, 2H), 6.64 (s, 1H), 7.16–7.18 (m, 1H), 7.35–7.46 (m, 10H), 7.93–7.94 (m, 1H), 8.13–8.16 (m, 1H), 8.18 (s, 1H), 8.22–8.24 (m, 1H), 9.93 (s, 1H).

*4.1.4. 2,4-bis(Benzyloxy)-5-isopropyl-N-(pyridin-4-yl)benzamide (**11**)*

The synthetic procedure for compound **11** is similar to that used for compound **10** and gave a yield of 70.83% as a white solid. ^{1}H NMR (500 MHz, $CDCl_3$): δ 1.27 (d, *J* = 7 Hz, 6H), 3.35 (qui, *J* = 7 Hz, 1H), 5.14 (s, 2H), 5.18 (s, 2H), 6.64 (s, 1H), 7.07–7.08 (m, 2H), 7.35–7.50 (m, 10H), 8.16 (s, 1H), 8.33–8.34 (m, 2H), 10.01 (s, 1H).

*4.1.5. tert-Butyl 5-(2,4-bis(benzyloxy)-5-isopropylbenzamido)-1H-indole-1-carboxylate (**13**)*

A mixture of 5-nitroindole (2 g, 12.33 mmol) was dissolved in DCM (15 ml) and added DMAP (3 g, 24.56 mmol) and Boc anhydride (4 g, 18.33 mmol) at R.T. for overnight. The reaction was quenched with water and extracted with EtOAc (30 ml x 3). The organic layer was collected and dried over anhydrous $MgSO_4$ concentrated *in*

vacuo and without more purification. The crude product was dissolved in IPA (100 ml) and H_2O (25 ml) and added iron powder (3.5 g, 63.64 mmol) and NH_4Cl (3 g, 55.56 mmol). The reaction was stirred and reflux for 1h. The iron powder was removed by methyl alcohol wash through celite packing. The organic layer was concentrated *in vacuo* and without more purification. Then the mixture of **9** (2 g, 5.31 mmol), EDC.HCl (1.5 g, 7.85 mmol), HOBt (0.9 g, 6.67 mmol), NMM (1.4 ml, 12.75 mmol) and DMF (8 ml) was stirred for 10 min then added crude product at R.T. for overnight, the reaction was quenched with water and extracted with EtOAc (30 ml x 3). The organic layer was collected and dried over anhydrous $MgSO_4$ concentrated *in vacuo* to yield colorless oil product. The residue was purified by silica gel chromatography (EtOAc:n-hexane = 1: 1, Rf = 0.6) to afford **13** (2.46 g, 78.59%) as a white solid. ^{1}H NMR (500 MHz, $CDCl_3$): δ 1.28 (d, J = 7.0 Hz, 6H), 1.16 (s, 9H), 3.36 (qui, J = 7.0 Hz, 1H), 5.15 (s, 4H), 6.45 (s, 1H), 6.46 (s, 1H), 6.80 (s, 1H), 7.34–7.52 (m, 11H), 7.91 (s, 2H), 8.24 (s, 1H), 9.95 (s, 1H).

4.1.6. 2,4-bis(Benzyloxy)-5-isopropyl-N-(1-methyl-1H-indol-5-yl) benzamide ***(14)***

A mixture of 5-nitroindole (2 g, 12.33 mmol), NaH (0.6 g, 15 mmol) and DMF (10 ml) was added methyl iodide (1.5 ml, 24.09 mmol) at R.T. for 2 h. The reaction was quenched with water and extracted with EtOAc (30 ml x 3). The organic layer was collected and dried over anhydrous $MgSO_4$ concentrated *in vacuo* and purified by silica gel chromatography (EtOAc:n-hexane = 1: 4, Rf = 0.2) to afford product as a yellow solid. The above product was dissolved in IPA (68 ml) and H_2O (17 ml) and added iron powder (2.5 g, 45.45 mmol) and NH_4Cl (2 g, 37.04 mmol). The reaction was stirred and reflux for 1 h. The iron powder was removed by a methyl alcohol wash through celite packing. The organic layer was concentrated *in vacuo* and without more purification. Then the mixture of **9** (2 g, 5.31 mmol), EDC.HCl (1.5 g, 7.85 mmol), HOBt (0.9 g, 6.67 mmol), NMM (1.4 ml, 12.75 mmol) and DMF (8 ml) was stirred for 10 min then added crude product at R.T. for overnight, the reaction was quenched with water and extracted with EtOAc (30 ml x 3). The organic layer was collected and dried over anhydrous $MgSO_4$ and concentrated *in vacuo* to yield a colorless oil product. The residue was purified by silica gel chromatography (EtOAc:n-hexane = 1: 2, Rf = 0.6) to afford **14** (0.96 g, 32.85%) as a white solid. ^{1}H NMR (500 MHz, $CDCl_3$): δ 1.28 (d, J = 7.0 Hz, 6H), 3.36 (qui, J = 7.0 Hz, 1H), 3.73 (s, 3H), 5.15 (s, 2H), 5.16 (s, 2H), 6.36 (d, J = 3.0 Hz, 1H), 6.62 (s, 1H), 7.02–7.05 (m, 2H), 7.11 (d, J = 8.5 Hz, 1H), 7.35 (t, J = 7.0 Hz, 1H), 7.40–7.53 (m, 10H), 7.70 (d, J = 1.5 Hz, 1H), 8.24 (s, 1H), 9.86 (d, 1H).

4.1.7. 1-(2,4-bis(Benzyloxy)phenyl)ethanone ***(16)***

A mixture of 1-(2,4-dihydroxyphenyl)ethanone (10 g, 65.77 mmol), benzyl bromide (18 ml, 151.33 mmol), potassium carbonate (28 g, 202.60 mmol) and acetone (250 ml) was refluxed overnight, the precipitate was filtered. The organic layer was collected and concentrated *in vacuo* to yield an oily product, and the oily product was added n-hexane and stirred overnight. The residue was filtered by suction filtration to yield white product and without more purification to afford **16** (20.43 g, 93.42%) as a white solid. ^{1}H NMR (500 MHz, $CDCl_3$): δ 2.55 (s, 3H), 5.09 (s, 2H), 5.11 (s, 2H), 6.60–6.62 (m, 2H), 7.34–7.43 (m, 10H), 7.84 (d, J = 9 Hz, 1H).

4.1.8. 2-(2,4-bis(Benzyloxy)phenyl)propan-2-ol ***(17)***

To a mixture of **16** (20 g, 60.17 mmol) and THF (100 ml) was added 3 M methylmagnesium bromide (33 ml) at 0 °C. The reaction was allowed back to R.T. and stirred for 4 h. The reaction was quenched with water at 0 °C.The residue was filtered by suction filtration to yield white product and without more purification to afford **17** (16.21 g, 77.30%) as a white solid.^{1}H NMR (500 MHz, $CDCl_3$): δ 1.53 (s, 3H), 1.59 (s, 3H), 3.98 (s, 1H), 5.04 (s, 2H), 5.10 (s, 2H), 6.53–6.55 (m, 1H), 6.67 (d, J = 2.5 Hz, 1H), 7.24 (d, 1H), 7.33–7.42 (m, 10H).

4.1.9. (((4-Isopropyl-1,3-phenylene)bis(oxy))bis(methylene)) dibenzene ***(18)***

To a mixture of **17** (16 g, 45.92 mmol) and CH_2Cl_2 (125 ml) was added triethylsilane (9 ml, 56.35 mmol) and TFA (4.5 ml, 58.77 mmol) at −78 °C. The reaction was allowed back to R.T. and stirred for 4 h. The reaction was quenched with 1 N NaOH (aq.) and extracted with CH_2Cl_2 (30 ml x 3). The organic layer was collected and dried over anhydrous $MgSO_4$ concentrated *in vacuo* to yield a colorless oil product. The residue was purified by silica gel chromatography (EtOAc:n-hexane = 1: 19, Rf = 0.35) to afford **18** (14.06 g, 92.08%) as a white solid.^{1}H NMR (500 MHz, $CDCl_3$): δ 1.25 (d, J = 6.5 Hz, 6H), 3.37 (Sep, J = 7.0 Hz, 1H), 5.05 (s, 2H), 5.07 (s, 2H), 6.58–6.60 (m, 1H), 6.63 (d, J = 2.5 Hz, 1H), 7.16 (d, J = 8.5 Hz, 1H), 7.34–7.47 (m, 10H).

4.1.10. 2,4-bis(Benzyloxy)-5-isopropylbenzaldehyde ***(19)***

A mixture of $POCl_3$ (3.3 ml, 35.40 mmol) and DMF (2.7 ml) was stirred at 0 °C for 10 min then added **18** (4 g, 12.03 mmol) dissolved in DMF (3 ml). The reaction was heated at 80 °C and stirred for 1.5 h. The reaction was quenched with 6 N NaOH (aq.) and extracted with EtOAc (30 ml x 3). The organic layer was collected and dried over anhydrous $MgSO_4$ concentrated *in vacuo* to yield a yellow product. The residue was without more purification to afford **19** (4.01 g, 92.40%) as a yellow solid.^{1}H NMR (500 MHz, $CDCl_3$): δ 1.21 (d, J = 7.0 Hz, 6H), 3.28 (Sep, J = 7.0 Hz, 1H), 5.10 (s, 2H), 5.12 (s, 2H), 6.50 (s, 1H), 7.34–7.42 (m, 10H), 7.74 (s, 1H), 10.39 (s, 1H).

4.2. Biology

4.2.1. Cell lines

The human non-small cell lung cancer cell line A549, human breast adenocarcinoma cell line MDA-MB-231, human colorectal carcinoma cell line HCT-116, human hepatoma cell line Hep3B and human umbilical vein endothelial cells (HUVEC) were obtained from Bioresource Collection and Research Center (Taiwan). Cells were maintained in RPMI-1640 medium, L-15 medium, McCoy's 5a medium and MEM medium supplemented with 10% (v/v) fetal bovine serum (Gibco, Carlsbad, CA, USA) and 1% of a mixture of penicillin-streptomycin-amphotericin B (Kibbutz Beit Haemek, Israel). Photoreceptor-derived 661W cells were the kind gift of Prof Muayyad Al-Ubaidi, University of Houston. Cells were maintained in DMEM high glucose medium supplemented with 10% (v/v) fetal bovine serum and 1% of a mixture of penicillin-streptomycin-amphotericin B.

4.2.2. Chemicals and antibodies

SRB (sulforodamine B) and MTT (3-(4,5-dimethylthiazol-2-yl)-2,5-diphenyltetrazolium bromide) were purchased from Sigma Chemical Co (St. Louis, MO, USA). Antibodies against Hsp90, FAK, p-FAK, p-Src, p-Rb, Akt, p-Akt, p-GSK3β, p-mTOR, 4EBP-1, p-4EBP-1, eIF-4E, p-p70S6K, EGFR, p-EGFR, MEK, p-MEK, ERK, p-ERK, p-cdc2 (Thr161), p-cdc2 (Tyr15), p-cdc2 (Ser216), caspase-9, caspase-3, cleaved caspase-3, p-H2AX (Ser139) and p-ERBB2 were obtained from Cell Signaling Technologies (Beverly, MA, USA). Antibodies against PARP, cyckin B1 and cdc25c were purchased from Santa Cruz Biotechnology (Santa Cruz, CA, USA). p-MPM2 and p-Histone 3 (Ser10) were purchased from Upstate Biotechnology Inc. (Temecula, CA, USA). Src and p-p53 (Ser46) were purchased from Abcam (Cambridge, MA, USA).

4.2.3. Cell toxicity and cell proliferation assays

Cell cytotoxicity was measured using a colorimetric MTT assay. 5×10^3 cells/well were seeded in a 96-well plate and then treated with the indicated concentrations of test compounds for 48 h. 0.5 mg/ml MTT solution was then added to the 96-well plate in the dark and the plate was incubated at 37 °C for 1.5 h. MTT-containing medium were removed and DMSO were added to each well to lyse cells, the absorbance was spectrophotometrically recorded at 570 nm.

Cell proliferation was measured using the sulforhodamine B (SRB) assay. 5×10^3 cells/well were incubated for 48 h with the indicated concentrations of test compounds, fixed with 10% trichloroacetic acid, stained for 30 min with SRB (0.4% in 1% acetic acid), and washed repeatedly with 1% acetic acid. Protein-bound dye was finally dissolved in 10 mM Tris base solution, and the optical density at 515 nm was measured.

4.2.4. Hsp90 enzyme activity assay

Enzyme inhibition assays were measured with a specific HSP90 enzyme activity assay (BPS Bioscience, San Diego, CA, USA). The assay is based on the competition of fluorescently labeled geldanamycin for binding to purified recombinant HSP90α. Briefly, all reagents were mixed per the instructions then added into wells and incubated at R.T. for 1–2 h with slow shaking. Fluorescent polarization of the sample in a microtiter-plate reader was read at excitation wavelengths ranging from 475 to 495 nm and detection of emitted light ranging from 518 to 538 nm.

4.2.5. Immunoblot and immunoprecipitation analyses

After treatment with the indicated conditions, cells were incubated for 10 min at 4 °C in lysis buffer (Cell Signaling Technology, Danvers, MA, USA), then scraped from the culture surface, incubated on ice for 10 min, and centrifuged for 30 min at 17,000 g and 4 °C. Protein samples were then electrophoresed on sodium dodecyl sulfate polyacrylamide gels and transferred onto nitrocellulose membranes, which were blocked by 5% milk in tris-buffered saline (TBS) for 1h at R.T.. Membranes were incubated with primary antibodies in TBS overnight at 4 °C, followed by incubation with hP-conjugated secondary antibodies for 1 h at R.T.. To measure bound antibodies, the membranes were treated with an enhanced chemiluminescence reagent (Advansta Corp., Menlo Park, CA, USA) and exposed to photographic film.

4.2.6. Cell migration assay

Cell migration was determined using a 24-well Boyden chamber with 12 μm pore size polycarbonate polyvinylpyrrolidone-free Nucleopore filters (Millipore, MA, USA). The membrane was coated with 0.5% gelatin for 4 h. First, 1×10^5 A549 cells were seeded in upper chamber and added 10% FBS medium as chemoattractant in the lower chamber. Both wells were treated with different drugs. After 6 h, the membranes were fixed with 4% formalin for 10 min and then stained with 1% crystal violet for 10 min. The cell number was counted using a microscope. Finally, the crystal violet on the membrane were dissolved with 0.1 M sodium citrate and detected with 550 nM wavelength.

4.2.7. Tumor xenograft model

8-week-old male BALB/c nude mice were fed water ad libitum and Pico-Lab Rodent Diet. All procedures were performed in accordance with the NIH guidelines on laboratory animal welfare. A549 or H1975 cells (1×10^7 cells) were subcutaneously injected into the flanks of mice. When tumor sizes reached 100 mm^3, mice were randomized into different groups with an indicated dosage of compound **6b** (dissolved in 1% carboxymethyl cellulose + 0.5% Tween 80 in D5W, p.o), STA-9090 (dissolved in DMSO/ethanol/Cremophor (1:4:5), ip, qwk, once weekly) and afatinib (dissolved in 1% carboxymethyl cellulose + 0.5% Tween 80 in D5W, po, daily) alone or a combination of both. Body weights and tumor sizes were measured twice a week. All mouse tumors were allowed to reach an endpoint volume of 2500 mm^3. Tumors were then dissected and subjected to further analysis.

4.2.8. Statistical analysis

All data were expressed as mean values ± S.E.M. and were measured independently three times. The significance of differences between the experimental groups and controls was assessed by Student's t-test. $P < 0.05$ was considered statistically significant ($*p < 0.05$; $**p < 0.01$; $***p < 0.001$; compared with the respective control group).

4.2.9. Inhibition effects on Cytochrome P450 in human liver microsomes

In direct CYP inhibition experiments, incubations were performed in triplicate in 96-well plates containing test compound and known positive control inhibitors. All incubations contained 0.1–1 mg/mL of pooled human liver microsomes (depending on which enzyme was assessed), 1 mM NADPH, and 2.5 mM $MgCl_2$ in 100 mM potassium phosphate buffer, pH 7.4. Eight concentrations of test article and positive control inhibitors or control solvent (DMSO) were added to the incubation. Final solvent concentration was 0.1% (v/v). Incubations were commenced with the addition of probe substrates to a final incubation volume of 200 μL and maintained at 37 °C for the defined period. Incubations were terminated by addition of methanol (200 μL). Aliquots of 30 μL terminated incubation mixtures were extracted by adding 3-fold volume of deprotein solvent (0.1% formic acid in methanol or acetonitrile) containing internal standard and centrifuged at 20000 g for 5 min. The supernatants were analyzed by LC-MS/MS.

4.2.10. Bidirectional Caco-2 permeability assay

Caco-2 cells were seeded at a density of 8×10^4 cells/cm^2 onto cell culture inserts with polycarbonate membrane for 21 days. For absorptive (AP → BL) permeability, transport was initiated by adding 0.4 mL of drug solution (HBSS/MES, pH 6.5 containing 10 μM test compound, 0.1% DMSO) to the apical chamber (donor chamber) of inserts bathed with 0.6 mL of transport medium (HBSS/HEPES, pH 7.4) in the basolateral chamber (receiver chamber). For secretory (BL→AP) permeability, transport was initiated by adding 0.6 mL of drug solution (HBSS/HEPES, pH 7.4 containing 10 μM test compound, 0.1% DMSO) to the basolateral chamber (donor chamber) of wells with 0.4 mL of transport medium (HBSS/MES, pH 6.5) in the apical chamber (receiver chamber). Samples (100 μL) were withdrawn from the receiver chamber at 30, 60, 90 and 120 min and from the donor chamber at 0 and 120 min. The volume withdrawn was replaced with fresh transport medium. The concentrations of test compound were analyzed by LC-MS/MS.

4.2.11. Pharmacokinetics study in male SD rats

Dose formulations were prepared on the dosing day prior to dosing. Vehicle for IV formulation consisted of 5% v/v N,N-dimethylacetamide (DMA) and 5% v/v Kolliphor® HS 15 (Solutol HS) in D5W (dextrose 5% in water solution). The vehicle for PO formulation consisted of 1% w/v carboxymethyl cellulose (CMC) and 0.5% v/v Tween 80. Complete mixing was ensured by stirring. The male Sprague Dawley rats were assigned to 2 dose groups of three animals each. Compound **6b** was administered to the study animals either intravenously (IV; Group 1) or orally by gavage (PO; Group 2) at the dose levels of 2 mg/kg (IV dosing) or 20 mg/kg (PO dosing). Blood samples were obtained pre-dose and at 0.03, 0.08, 0.25, 0.5, 1, 2, 4, 6, 8, 12 and 24 h post-dose from the animals in

Group 1, and pre-dose and at 0.25, 0.5, 1, 2, 4, 6, 8, 12, 24, 48 and 72 h post-dose from the animals in Group 2. Blood samples were processed to plasma within 60 min after collection. Plasma samples were analyzed at QPS Taiwan using an LC-MS/MS method. Individual concentration-time data were used in the calculation of PK parameters of compound **6b** using Phoenix® WinNonlin® version 6.3.

4.2.12. In vitro hepatocytes stability

The metabolism of **6b** was investigated in cryopreserved hepatocytes from CD-1 mice, Sprague-Dawley rat, Beagle dog and human. Incubations of **6b** (10 μM) and hepatocytes were conducted in 12-well plates containing approximately 0.5×10^6 cells/well in triplicate for 4 h at 37 °C with 90–120 rpm orbital shaking. Metabolic reactions were stopped at 0.5, 1, 2 and 4 h by adding 1x volume of acetonitrile. The test article depletion and metabolite identification were performed using a QTRAP 5500 LC-MS/MS system (AB SCIEX). Multiple reaction monitoring, precursor ion, neutral loss, and glucuronide neutral loss scans in positive ion electrospray mode were used to identify compound **6b** and its metabolites.

4.2.13. The hERG human potassium channel assay

This assay measures binding of [^{3}H] labeled Astemizole to potassium channel hERG. Briefly, HEK-293 cells stably transfected with a plasmid encoding the human potassium channel hERG are used to prepare membranes in modified HEPES pH 7.4 buffer. A 10 μg aliquot of membrane is incubated with 1.5 nM [^{3}H]Astemizole for 60 min at 25 °C. Non-specific binding is estimated in the presence of 10 μM Astemizole. Membranes are filtered and washed 3 times and the filters are counted to determine [^{3}H]Astemizole specifically bound.

Declaration of competing interest

The authors declare that they have no known competing financial interests or personal relationships that could have appeared to influence the work reported in this paper.

Acknowledgment

This paper is dedicated to the memory of our dear supervisor Professor Che-Ming Teng (Pharmacological Institute, College of Medicine, National Taiwan University), who passed away recently. Professor Teng took part in the study design and the provided critical supervision for the experiments. We thank Prof. Muayyad Al-Ubaidi from University of Houston for providing photoreceptor-derived 661W cells. This research was supported by the Ministry of Science and Technology, Taiwan (grant no. MOST 108-2113-M-038 -005 and MOST 109-2113-M-038 -005).

Appendix A. Supplementary data

Supplementary data to this article can be found online at https://doi.org/10.1016/j.ejmech.2021.113428.

References

[1] L. Whitesell, S.L. Lindquist, HSP90 and the chaperoning of cancer, Nat. Rev. Canc. 5 (2005) 761–772.
[2] S.D. Gupta, M.K. Bommaka, A. Banerjee, Inhibiting protein-protein interactions of Hsp90 as a novel approach for targeting cancer, Eur. J. Med. Chem. 178 (2019) 48–63.
[3] Z. Solárová, J. Mojžiš, P. Solár, Hsp90 inhibitor as a sensitizer of cancer cells to different therapies (review), Int. J. Oncol. 46 (2015) 907–926.
[4] H. Mellatyar, S. Talaei, Y. Pilehvar-Soltanahmadi, A. Barzegar, A. Akbarzadeh, A. Shahabi, M. Barekati-Mowahed, N. Zarghami, Targeted cancer therapy through 17-DMAG as an Hsp90 inhibitor: overview and current state of the art, Biomed. Pharmacother. 102 (2018) 608–617.
[5] R.C. Schnur, M.L. Corman, R.J. Gallaschun, B.A. Cooper, M.F. Dee, J.L. Doty, M.L. Muzzi, C.I. DiOrio, E.G. Barbacci, P.E. Miller, V.A. Pollack, D.M. Savage, D.E. Sloan, L.R. Pustilnik, J.D. Moyer, M.P. Moyer, erbB-2 oncogene inhibition by geldanamycin derivatives: synthesis, mechanism of action, and structure-activity relationships, J. Med. Chem. 38 (1995) 3813–3820.
[6] S.R. Kasibhatla, K. Hong, M.A. Biamonte, D.J. Busch, P.L. Karjian, J.L. Sensintaffar, A. Kamal, R.E. Lough, J. Brekken, K. Lundgren, R. Grecko, G.A. Timony, Y. Ran, R. Mansfield, L.C. Fritz, E. Ulm, F.J. Burrows, M.F. Boehm, Rationally designed high-affinity 2-amino-6-halopurine heat shock protein 90 inhibitors that exhibit potent antitumor activity, J. Med. Chem. 50 (2007) 2767–2778.
[7] P.A. Brough, W. Aherne, X. Barril, J. Borgognoni, K. Boxall, J.E. Cansfield, K.-M.J. Cheung, I. Collins, N.G.M. Davies, M.J. Drysdale, B. Dymock, S.A. Eccles, H. Finch, A. Fink, A. Hayes, R. Howes, R.E. Hubbard, K. James, A.M. Jordan, A. Lockie, V. Martins, A. Massey, T.P. Matthews, E. McDonald, C.J. Northfield, L.H. Pearl, C. Prodromou, S. Ray, F.I. Raynaud, S.D. Roughley, S.Y. Sharp, A. Surgenor, D.L. Walmsley, P. Webb, M. Wood, P. Workman, L. Wright, 4,5-Diarylisoxazole HSP90 chaperone inhibitors: potential therapeutic agents for the treatment of cancer, J. Med. Chem. 51 (2008) 196–218.
[8] T.-Y. Lin, M. Bear, Z. Du, K.P. Foley, W. Ying, J. Barsoum, C. London, The novel HSP90 inhibitor STA-9090 exhibits activity against Kit-dependent and –independent malignant mast cell tumors, Exp. Hematol. 36 (2008) 1266–1277.
[9] A.J. Woodhead, H. Angove, M.G. Carr, G. Chessari, M. Congreve, J.E. Coyle, J. Cosme, B. Graham, P.J. Day, R. Downham, L. Fazal, R. Feltell, E. Figueroa, M. Frederickson, J. Lewis, R. McMenamin, C.W. Murray, M.A. O'Brien, L. Parra, S. Patel, T. Phillips, D.C. Rees, S. Rich, D.M. Smith, G. Trewartha, M. Vinkovic, B. Williams, A.J. Woolford, Discovery of (2,4-dihydroxy-5-isopropylphenyl)-[5-(4-methylpiperazin-1-ylmethyl)-1,3-dihydroisoindol-2-yl]methanone (AT13387), a novel inhibitor of the molecular chaperone Hsp90 by fragment based drug design, J. Med. Chem. 53 (2010) 5956–5969.
[10] (a) S. Jung, N.G. Yoon, S. Yang, D. Kim, W.S. Lee, K.B. Hong, C. Lee, B.H. Kang, J.H. Lee, S. Kang, Discovery of 2-((4-resorcinol)-5-aryl-1,2,3-triazol-1-yl)acetates as potent Hsp90 inhibitors with selectivity over TRAP1, Bioorg. Med. Chem. Lett 30 (2020) 126809;
(b) C. Liang, X. Wu, Z. Li, J. Zhu, C. Lu, Y. Shen, Design, synthesis and pharmacological evaluation of N-(5-chloro-2,4-dihydroxybenzoyl)-(R)-N-arylmethyl-1,2,3,4-tetrahydro-3-isoquinolinecarboxamides as potent Hsp90 inhibitors, Eur. J. Med. Chem. 143 (2018) 85–96;
(c) K. Nepali, M.H. Lin, M.W. Chao, S.J. Peng, K.C. Hsu, T. Eight Lin, M.C. Chen, M.J. Lai, S.L. Pan, J.P. Liou, Amide-tethered quinoline-resorcinol conjugates as a new class of HSP90 inhibitor suppressing the growth of prostate cancer cells, Bioorg. Chem. 91 (2019) 103119;
(d) S.Y. Park, Y.J. Oh, Y. Lho, J.H. Jeong, K.H. Liu, J. Song, S.H. Kim, E. Ha, Y.H. Seo, Design, synthesis, and biological evaluation of a series of resorcinol-based N-benzyl benzamide derivatives as potent Hsp90 inhibitors, Eur. J. Med. Chem. 143 (2018) 390–401.
[11] (a) M. Wang, A. Shen, C. Zhang, Z. Song, J. Ai, H. Liu, L. Sun, J. Ding, M. Geng, A. Zhang, Development of heat shock protein (Hsp90) inhibitors to combat resistance to tyrosine kinase inhibitors through hsp90-kinase interactions, J. Med. Chem. 59 (2016) 5563–5586;
(b) A. Courtin, T. Smyth, K. Hearn, H.K. Saini, N.T. Thompson, J.F. Lyons, N.G. Wallis, Emergence of resistance to tyrosine kinase inhibitors in non-small-cell lung cancer can be delayed by an upfront combination with the HSP90 inhibitor onalespib, Br. J. Canc. 115 (2016) 1069–1077.
[12] (a) J. Han, L.A. Goldstein, W. Hou, S. Chatterjee, T.F. Burns, H. Rabinowich, HSP90 inhibition targets autophagy and induces a CASP9-dependent resistance mechanism in NSCLC, Autophagy 14 (2018) 958–971;
(b) S. Cedrés, E. Felip, C. Cruz, A. Martinez de Castro, N. Pardo, A. Navarro, A. Martinez-Marti, J. Remon, J. Zeron-Medina, J. Balmaña, A. Llop-Guevara, J.M. Miquel, I. Sansano, P. Nuciforo, F. Mancuso, V. Serra, A. Vivancos, Activity of HSP90 inhibiton in a metastatic lung cancer patient with a germline BRCA1 mutation, J. Natl. Cancer Inst. 110 (2018) 914–917.
[13] E. Kurihara, K. Shien, H. Torigoe, T. Takeda, Y. Takahashi, Y. Ogoshi, T. Yoshioka, K. Namba, H. Sato, K. Suzawa, H. Yamamoto, J. Soh, M. Okazaki, T. Shien, S. Tomida, S. Toyooka, Ganetespib in epidermal growth factor receptor-tyrosine kinase inhibitor-resistant non-small cell lung cancer, Anticancer Res. 39 (2019) 1767–1775.
[14] A. Akram, S. Khalil, S.A. Halim, H. Younas, S. Iqbal, S. Mehar, Therapeutic uses of HSP90 inhibitors in non-small cell lung carcinoma (NSCLC), Curr. Drug Metabol. 19 (2018) 335–341.
[15] E. Felip, F. Barlesi, B. Besse, Q. Chu, L. Gandhi, S.W. Kim, E. Carcereny, L.V. Sequist, P. Brunsvig, C. Chouaid, E.F. Smit, H.J.M. Groen, D.W. Kim, K. Park, E. Avsar, S. Szpakowski, M. Akimov, E.B. Garon, Phase 2 study of the HSP-90 inhibitor AUY922 in previously treated and molecularly defined patients with advanced non-small cell lung cancer, J. Thorac. Oncol. 13 (2018) 576–584.
[16] Z. Piotrowska, D.B. Costa, G.R. Oxnard, M. Huberman, J.F. Gainor, I.T. Lennes, A. Muzikansky, A.T. Shaw, C.G. Azzoli, R.S. Heist, L.V. Sequist, Activity of the

Hsp90 inhibitor luminespib among non-small-cell lung cancers harboring EGFR exon 20 insertions, Ann. Oncol. 29 (2018) 2092–2097.
[17] T. Shimamura, S.A. Perera, K.P. Foley, J. Sang, S.J. Rodig, T. Inoue, L. Chen, D. Li, J. Carretero, Y.C. Li, P. Sinha, C.D. Carey, C.L. Borgman, J.P. Jimenez, M. Meyerson, W. Ying, J. Barsoum, K.K. Wong, G.I. Shapiro, Ganetespib (STA-9090), a nongeldanamycin HSP90 inhibitor, has potent antitumor activity in in vitro and in vivo models of non-small cell lung cancer, Clin. Canc. Res. 18 (2012) 4973–4985.